

This is a repository copy of *Incorporation of boron into metakaolin-based geopolymers for radionuclide immobilisation and neutron capture potential*.

White Rose Research Online URL for this paper: <a href="https://eprints.whiterose.ac.uk/id/eprint/232926/">https://eprints.whiterose.ac.uk/id/eprint/232926/</a>

Version: Published Version

# Article:

Niu, X., Elakneswaran, Y., Li, A. et al. (6 more authors) (2025) Incorporation of boron into metakaolin-based geopolymers for radionuclide immobilisation and neutron capture potential. Cement and Concrete Research, 190. 107814. ISSN: 0008-8846

https://doi.org/10.1016/j.cemconres.2025.107814

# Reuse

This article is distributed under the terms of the Creative Commons Attribution-NonCommercial (CC BY-NC) licence. This licence allows you to remix, tweak, and build upon this work non-commercially, and any new works must also acknowledge the authors and be non-commercial. You don't have to license any derivative works on the same terms. More information and the full terms of the licence here: https://creativecommons.org/licenses/

# **Takedown**

If you consider content in White Rose Research Online to be in breach of UK law, please notify us by emailing eprints@whiterose.ac.uk including the URL of the record and the reason for the withdrawal request.



ELSEVIER

Contents lists available at ScienceDirect

# Cement and Concrete Research

journal homepage: www.elsevier.com/locate/cemconres





# Incorporation of boron into metakaolin-based geopolymers for radionuclide immobilisation and neutron capture potential

Xiaobo Niu<sup>a,\*</sup>, Yogarajah Elakneswaran<sup>a,\*</sup>, Ang Li<sup>a</sup>, Sivasubramaniam Seralathan<sup>a</sup>, Ryosuke Kikuchi<sup>a</sup>, Yoshihisa Hiraki<sup>b</sup>, Junya Sato<sup>b</sup>, Takeshi Osugi<sup>b</sup>, Brant Walkley<sup>c</sup>

- a Division of Sustainable Resources, Graduate School of Engineering, Hokkaido University, North 13, West 8, Sapporo 060-8628, Hokkaido, Japan
- b Waste Treatment Technology Section, Decommissioning Technology Department, Nuclear Backend Technology Center, Nuclear Fuel Cycle Engineering Laboratories, Japan Atomic Energy Agency, Japan
- c School of Chemical, Materials and Biological Engineering, The University of Sheffield, Sir Robert Hadfield Building, Mappin Street, Sheffield S1 3JD, UK

#### ARTICLE INFO

# Keywords: Metakaolin-based geopolymer Boron Alkali-activated materials Acid-activated materials Borosilicate Radionuclides Immobilisation

#### ABSTRACT

Metakaolin-based geopolymers have attracted significant interest in decontaminating radioactive debris from the Fukushima nuclear accident. This study explored the incorporation of boron (B) into geopolymers using boric acid as the source, with the goal of developing B-enriched geopolymers for enhanced radionuclide immobilisation and neutron capture potential. The addition of boric acid lowered the pH of the alkali activator, reducing metakaolin solubility and impeding alkali-activated geopolymerisation. B formed an unstable BO<sub>4</sub>(xB, 4-xSi) structure with extra short-range Si tetrahedra in low-temperature curing conditions, making it prone to be leached out. High-temperature curing facilitated alkali-activated geopolymerisation, mitigating some negative effects of boric acid. It also promoted partial incorporation of BO4 into the framework, reducing leaching. Additionally, in acid-activated geopolymers, boric acid absorbed substantial reaction heat during the initial dealumination phase by reacting with PO<sub>4</sub>, thereby enhancing the overall geopolymerisation degree and increasing the relative content of near-Si terminal P and Al<sub>6</sub> units. B could be incorporated into the framework by bonding with numerous Al-unsaturated Si tetrahedra to form a stable BO<sub>4</sub>(0B, 4Si) structure. Although B introduction slightly reduced the positive charge of the acid-activated geopolymer's structure, decreasing its capacity to immobilise anionic SeO<sub>3</sub><sup>2-</sup> through electrostatic adsorption, the decrease was negligible. Conversely, B introduction increased structural compactness, which improved Cs<sup>+</sup> immobilisation through physical entrapment. Overall, the B-containing acid-activated geopolymer effectively incorporated B into the main matrix while maintaining radionuclide immobilisation capacity. This study provides valuable insights into the selection and incorporation mechanisms of the B-containing geopolymer matrix, contributing to effective strategies for radioactive waste disposal.

#### 1. Introduction

During the decommissioning phase following the Fukushima Daiichi (1F) incident, a substantial amount of radioactive waste was generated and contained on-site [1]. This waste mainly consisted of fuel debris within the primary containment vessels (PCVs) of Fukushima Daiichi Units 1, 2, and 3, along with contaminated water produced after the cooling process ceased [2]. Currently, the Tokyo Electric Power Company (TEPCO) and the Japan Atomic Energy Agency (JAEA) primarily focus on managing solid waste resulting from molten core-concrete interactions (MCCI), as well as slurry and sediment wastes containing

colloidal substances [3–5]. These radioactive residues are rich in radionuclides generated from fission reactions within reactors, accelerators, or neutron generators, including Cs-137, Sr-90, Co-60, Se-79, and I-131 [6–9]. Simultaneously, these residues emit significant neutron radiation, which presents substantial challenges for detection and shielding due to their electrically neutral nature [10,11]. Furthermore, neutron radiation is highly hazardous to environmental and human health, as it can transmute elements in the body into radioactive isotopes, causing internal irradiation and severe acute radiation injuries, such as hematopoietic failure, gastrointestinal damage, and central nervous system disorders. Exposure to neutrons and gamma rays may

E-mail addresses: niuxiaobo@eng.hokudai.ac.jp (X. Niu), elakneswaran@eng.hokudai.ac.jp (Y. Elakneswaran).

https://doi.org/10.1016/j.cemconres.2025.107814

<sup>\*</sup> Corresponding authors.

also alter genetic material, potentially affecting offspring and exacerbating radiation effects [12-16].

Boron (B) is extensively used in neutron absorption, primarily due to the high neutron capture cross-section of its isotope B-10. This property enables the efficient absorption of thermal neutrons, resulting in the generation of Li-7 and  $\alpha$  particles (Eq. 1) [17,18]. The utilisation of B is prevalent in the cooling systems of nuclear reactors, typically in forms such as boric acid and boron carbide. These compounds, incorporated into control rods and other protective materials, are crucial in regulating nuclear reaction rates, preventing reactor overheating or runaway reactions, mitigating the risk of unintended chain reactions, and ensuring the sustained and safe operation of reactors [19–21]. Beyond its applications in nuclear energy, boron's neutron capture capability is also harnessed in the medical field, particularly in Boron Neutron Capture Therapy (BNCT), with advancements in this technique further validating the effectiveness of boron in neutron absorption [22].

$$^{10}B + n \rightarrow ^{7}Li(0.84MeV) + \alpha(1.47MeV)$$
 (1)

Recently, several studies have focused on enhancing the neutron shielding and capture capabilities of cementitious materials utilised in nuclear applications. By incorporating boron-containing aggregates into Portland-cement-based concretes, these efforts have significantly enhanced the neutron shielding efficiency of these materials [23–25]. While these cement-based materials exhibit excellent mechanical properties and improved neutron shielding efficiency, their use in nuclear waste disposal applications is limited. This limitation arises due to their incompatibility with certain radionuclides and their high free water content, which can lead to problematic hydrogen generation [26–28]. In addition, although the shielding efficiency increases with the amount of boron-containing aggregates, an excessive amount can destabilise the cement matrix structure [24,25]. Therefore, it is necessary to explore more suitable matrix materials and to further understand the effect of boron content on matrix stability.

Geopolymers have garnered significant attention as promising encapsulation materials for nuclear waste disposal. As a viable alternative to conventional cementitious materials like Portland cement, geopolymers offer a unique three-dimensional network structure characterised by high density, low permeability, superior mechanical strength, excellent thermal stability, and remarkable fire and chemical corrosion resistance. [29]. Alkali activation, a highly efficient method for synthesising geopolymers, has become a key research focus. The geopolymerisation process involves the depolymerisation and polycondensation of an aluminosilicate precursor, such as fly ash or metakaolin, in the presence of a strong alkaline activator, resulting in a robust gel network [30,31]. Alkali-activated geopolymers are increasingly recognised for their potential in the long-term immobilisation of radionuclides in nuclear waste [32,33]. These geopolymers possess a permanently negatively charged surface due to their high density of tetrahedral aluminium sites, making them highly effective for the adsorption and immobilisation of cationic radionuclides [34-39]. Studies have shown that cationic radionuclides like Cs<sup>+</sup>, Sr<sup>2+</sup>, and Co<sup>2+</sup> are effectively immobilised in alkali-activated geopolymers through a multi-ion exchange mechanism [40]. Additionally, Cs<sup>+</sup> forms stable complexes with zeolites in the alkaline environment, ensuring secure immobilisation [41], while  $Sr^{2+}$  immobilisation has been demonstrated through the encapsulation of  $Sr^{2+}$ -loaded titanate ion exchangers [42]. Despite challenges in adsorbing and immobilising anionic radionuclides due to the negative surface charge, research suggests that the in-situ formation of ettringite could enhance the capacity for adsorbing and solidifying Se oxyanions [43]. In contrast to alkali activation, acidactivated geopolymers, particularly those activated by phosphoric acid, have emerged as a promising alternative. The acid-activation process involves the dealumination of an aluminosilicate precursor within a phosphoric acid activator, followed by the condensation of silicate tetrahedrons, forming P(OAl)<sub>x</sub>(H<sub>2</sub>O)<sub>4-x</sub> units connected to Si or

Al [44,45]. Acid activators require lower activation temperatures and produce fewer  $CO_2$  emissions compared to alkaline activators, like sodium hydroxide or silicate solutions [46]. Acid-activated geopolymers also exhibit superior mechanical properties compared to alkali-activated geopolymers [47], and their potential for the treatment of radioactive waste is being increasingly appreciated. Previous studies have shown that acid-activated geopolymers have pH-regulated surface charges, with positively charged surfaces in the pH range typical of geological nuclear waste disposal environments, enabling effective immobilisation of anionic radionuclides such as  $SeO_3^{2-}$ ,  $SeO_4^{2-}$ ,  $I^-$ , and  $IO_3^{-}$  [48].

However, both types of geopolymers lack structures that can efficiently capture uncharged neutrons from radioactive waste [49]. Several studies have investigated enhancing the neutron capture properties of geopolymers by incorporating boron carbide (B<sub>4</sub>C) as a neutron absorber [50,51]. While B<sub>4</sub>C is effective at neutron capture, it presents significant challenges, including difficulty in sintering—requiring temperatures above 2000 °C-and a tendency to remain as aggregates rather than integrating seamlessly into the aluminosilicate structure of geopolymers, which significantly reduces the effective cross-sectional area for neutron capture. These factors continue to limit the overall effectiveness of this approach. Additionally, comprehensive studies on successfully incorporating boron into both alkali-activated and acidactivated geopolymers to enhance their neutron capture properties are still lacking. Further research is crucial to understand the interaction between boron and the geopolymer matrix in both systems, with the goal of developing advanced borosilicate geopolymers that offer improved neutron absorption capabilities.

The aim of this study is to develop a method for incorporating boric acid as a B source into metakaolin-based geopolymers, enhancing their neutron capture capability while preserving their ability to immobilise radionuclides. It focuses on determining the form and stability of the incorporated B and investigating the structural modifications within the geopolymers following B incorporation. Geopolymers synthesised via both alkali and acid activation methods were systematically compared under different curing conditions. Structural changes due to varying B content were analysed using mechanical strength tests, X-ray diffraction (XRD), scanning electron microscopy (SEM), solid state nuclear magnetic resonance spectroscopy (NMR), and Fourier transform infrared spectroscopy (FTIR). The stability of B within the geopolymer matrix, along with its effects on the overall structural integrity and its radionuclide immobilisation capacity, was assessed using leaching tests and assessment of the leachate with inductively coupled plasma optical emission spectroscopy (ICP-OES). This comprehensive analysis enhances the understanding of B incorporation into metakaolin-based geopolymers and supports the development of borosilicate structures, offering valuable technical insights and potential applications in nuclear waste disposal, particularly in neutron-rich circumstances.

### 2. Experimental details

# 2.1. Materials

Metakaolin (#13-SF-7), with an average particle size (D50) of 1.08  $\mu m$ , obtained from Sobue Clay Co. Ltd. (Japan), was used for the synthesis of geopolymers. The chemical composition of metakaolin, determined by X-ray fluorescence (XRF), is listed in Table 1 with a Si:Al molar ratio of approximately 0.975. A potassium silicate solution (WAKO), containing 29.1 wt% SiO\_2, 21.9 wt% K\_2O and 49.0 wt% H\_2O, potassium hydroxide (WAKO, 86 wt% KOH), and ultrapure water were used to prepare the potassium silicate alkali-activator solution. Analytical-grade phosphoric acid (WAKO, 85 wt%  $\rm H_3PO_4$ ) and ultrapure water were used to prepare the phosphoric acid-activator solution. Boric acid (WAKO, 99.5%  $\rm + B_3(OH)_3)$  was used as the B source introduced into the geopolymers. Additionally,  $\rm K_2SeO_3$  and  $\rm CsNO_3$ , purchased from WAKO, were selected as the simulated radionuclide sources to prepare waste form samples.

Table 1
Chemical composition (wt%) of the metakaolin as determined by X-ray fluorescence.

Component	Metakaolin
SiO <sub>2</sub>	52.26
$Al_2O_3$	45.50
$Fe_2O_3$	0.45
TiO <sub>2</sub>	1.12
CaO	0.08
MgO	0.05
K <sub>2</sub> O	0.09
Na <sub>2</sub> O	0.09
$P_2O_5$	0.12
L.O.I.*	0.23

<sup>\*:</sup> L.O.I. is loss on ignition at 1100 °C for 12 h.

#### 2.2. Geopolymer samples synthesis

Alkali-activated geopolymers were synthesised by mechanically mixing stoichiometric amounts of metakaolin with sufficient quantities of alkali-activator solutions, resulting in a final chemical composition (in ceramic nomenclature) of 1K<sub>2</sub>O: 1Al<sub>2</sub>O<sub>3</sub>: 1SiO<sub>2</sub>: 13H<sub>2</sub>O. Acid-activated geopolymers were prepared similarly by mixing metakaolin with adequate amounts of acid-activator solutions, achieving a solid-to-liquid mass ratio of 1. The acid-activator solution was prepared by diluting 85 wt% phosphoric acid to 68 wt% (10.3 M H<sub>3</sub>PO<sub>4</sub>). Two curing conditions were employed for the alkali-activated geopolymers: low-temperature curing at 20 °C for 28 days (hereafter referred to as LT) and hightemperature curing at 60 °C for 6 days, followed by 1 day at room temperature (25  $^{\circ}$ C  $\pm$  1) (hereafter referred to as HT). A two-stage curing process was utilised for the acid-activated geopolymers, following a previously established method [48]. This involved precuring at 40 °C for 24 h, followed by curing at 60 °C for 24 h. Boric acid was externally incorporated at 1, 3 and 5 wt% of the geopolymer matrix. The boric acid was added to the activators and allowed to equilibrate for one day prior to mixing, and the pH of the activators was measured by a pH meter (AS ONE Ltd., Japan) before mixing. Samples were labelled based on the amount of boric acid added, curing conditions, and activation method, as shown in Table 2. Additionally, to prepare wasteform samples with simulated radionuclides, K<sub>2</sub>SeO<sub>2</sub> or CsNO<sub>3</sub> was separately added to the activator at a concentration of 1 mmol of the target ion per 100 g of geopolymer sample, followed by a

**Table 2**Activator information, curing conditions, and activation method adopted for the geopolymer samples with varying B content.

Samples	Boric acid (wt %)	Si/(B + Al)	Equilibrated activator pH	Curing conditions	Activation method
LT 0	0 1	1.475 1.404	$15.20 \pm 0.1$ $15.11 \pm 0.05$	20 °C 20 °C	Alkali Alkali
LT 3	3	1.282	$15.08 \pm 0.09$	20 °C	Alkali
LT 5	5	1.180	$14.90\pm0.07$	20 °C	Alkali
HT 0	0	1.475	$15.20\pm0.05$	60 °C + 20 °C	Alkali
HT 1	1	1.404	$15.11\pm0.04$	60 °C + 20 °C	Alkali
НТ 3	3	1.282	$15.08\pm0.07$	60 °C + 20 °C	Alkali
HT 5	5	1.180	$14.90 \pm 0.08$	60 °C + 20 °C	Alkali
Acid 0	0	0.975	$0.557\pm0.08$	40 °C + 60 °C	Acid
Acid 1	1	0.940	$0.560\pm0.06$	40 °C + 60 °C	Acid
Acid 3	3	0.878	$0.558\pm0.05$	40 °C + 60 °C	Acid
Acid 5	5	0.823	$0.561\pm0.03$	40 °C + 60 °C	Acid

24-h equilibration period before use. Finally, all samples for structural characterisation were dried in a thermostat at 40  $^{\circ}C$  for 24 h, then ground to a particle size of  $<\!150~\mu m$ .

#### 2.3. Compressive strength measurement

The compressive strength of hardened geopolymer samples was measured in accordance with the JIS A 1108 standard [52]. Cylindrical specimens with dimensions of  $\Phi 50~mm \times 40~mm$  were used for the measurements, as specified by the testing equipment. The compressive strength was calculated using Eq. 2.

$$f_c = \frac{P}{\pi \times \left(\frac{d}{2}\right)^2} \tag{2}$$

Where  $f_c$  represents the compressive strength in  $N/mm^2$ , P is the maximum load in N, and d is the specimen diameter in mm.

#### 2.4. Structural characterisation

A MultiFlex X-ray diffractometer (Rigaku, Japan) was used to characterise the geopolymer samples, employing CuKa radiation and scanning over a  $2\theta$  range of  $5^{\circ}$  to  $70^{\circ}$  with a scan speed of  $6.5^{\circ}$  per minute and a step size of 0.02°. Solid-state magic angle spinning (MAS) nuclear magnetic resonance (NMR) spectra of the geopolymer samples were obtained using a Bruker 500 MHz spectrometer equipped with an 11.74 T magnet. The <sup>11</sup>B MAS NMR spectra were recorded at 53.7 MHz using a 3.2 mm probe with a 2 µs (30°) pulse width, a spinning speed of 15 kHz, and a total of 720 scans with a 5 s recycle delay per sample. The <sup>29</sup>Si MAS NMR spectra were acquired at 99.4 MHz using a 3.2 mm probe with a 1.5 µs (30°) pulse width, a spinning speed of 5 kHz, and a total of 2800 scans with a 20 s recycle delay per sample. For <sup>27</sup>Al MAS NMR, a 2.5 mm probe operating at 130.4 MHz was used, with pulse widths of 2.4 µs for metakaolin, 3 µs for alkali-activated geopolymers, and 2.08 µs for acidactivated geopolymers (all 90° pulses), spinning at 30 kHz. A total of 3600 scans were recorded for each sample with a 5 s recycle delay. The  $^{31}\mathrm{P}$  MAS NMR spectra were recorded at 202.4 MHz using a 2.5 mm probe with a 3.2 µs (90°) pulse width, spinning at 30 kHz, with a total of 128 scans and a 5 s recycle delay per sample. Chemical shifts for <sup>11</sup>B, <sup>29</sup>Si, <sup>27</sup>Al, and <sup>31</sup>P nuclei were referenced to NaBH<sub>4</sub>, C<sub>6</sub>H<sub>18</sub>O<sub>3</sub>Si<sub>3</sub>, AlCl<sub>3</sub> solution (1 mol/L), and (NH<sub>4</sub>)H<sub>2</sub>PO<sub>4</sub>, respectively. The deconvolution of the <sup>29</sup>Si MAS NMR spectra employed the Gaussian amplitude function, while the deconvolution of the <sup>11</sup>B and <sup>27</sup>Al MAS NMR spectra accounted for their quadrupolar interactions and utilised a combination of multiple Pearson IV functions [53]. The morphology of all the samples was examined by scanning electron microscopy (SEM: JSM-IT200, JEOL, Japan) with a 25 kV acceleration voltage. The surfaces of all the samples were coated with Au at 20 mA for 120 s. The chemical bonding information of the sample was characterised through Fouriertransform infrared (FTIR) spectroscopy (JASCO670, Japan) with a constant spectral resolution of 4 cm<sup>-1</sup>. The zeta potential of the acid group samples was measured using a zeta potential and particle size analyser (ELSZ-1000ZS) in neutral (pH 7), acidic, and alkaline (pH 3-11) solutions with an ionic strength of 10 mM. The suspension's solidto-liquid ratio was maintained at 1 g/L. To adjust the ionic strength, KNO<sub>3</sub> was used, while KOH and HNO<sub>3</sub> were employed to control the pH levels.

# 2.5. Leaching experiments

The samples for the leaching experiments were prepared by pouring the fresh mixture into cylindrical moulds with a height of 1.5 cm and an internal diameter of 1.3 cm, resulting in a surface area of 8.8 cm<sup>2</sup>. The specimens were then sealed with parafilm and cured under consistent conditions according to their respective groups. After curing, static and

semi-dynamic leaching tests were conducted separately in accordance with the ANSI/ANS-16.1-2003 standard (American Nuclear Society, 2004) [54] at ambient temperature. Each specimen was immersed in 88 mL of deionised water as the leachant, maintaining a leachant volume-to-surface area ratio of 10 mL/cm². In the static group, leachates were collected at 2 and 9 h, and at 1, 3, 5, 7, and 14 days without replacing the leachant. In the semi-dynamic group, leachants were completely replaced at the same intervals after cumulative leaching times of 2 and 9 h, and 1, 3, 5, 7, and 14 days from the start of the test. The leachates were then analysed using inductively coupled plasma atomic emission spectroscopy (ICP-AES; SPECTROBLUE, Hitachi, Japan). The ICP-AES analysis covered the wavelength range of 165–770 nm, and all solutions used for ICP-AES measurements were spiked with 1% HNO<sub>3</sub> (~60 wt%) to protect the samples. The cumulative leaching rate (C) for the semi-dynamic group was calculated using Eq. 3.

$$C = \frac{A_t}{A_0} = \frac{1}{A_0 M} \sum_{i=0}^{t} C_i \times V$$
 (3)

where  $A_t$  [mmol] is the cumulative number of moles of leachable ions measured in the leachate during the test period,  $A_O$  [mmol] is the total number of moles of ions in the geopolymer sample for the leaching test, M is the relative molecular mass of the measured element,  $C_i$  [ppm] is the concentration of leached ions in each leaching section, and V [L] is the volume of the leachate.

#### 3. Results and discussion

#### 3.1. Mechanical properties of samples

Fig. 1 shows the compressive strength of three groups of geopolymer samples with varying B contents. When no boric acid was added, the LT group samples exhibited the highest average compressive strength. In contrast, the compressive strength of the HT group, derived from the same alkali-activated geopolymer but cured at a higher temperature, decreased by over 50%. This reduction in compressive strength under elevated curing temperatures is generally attributed to the accelerated geopolymerisation process, which induces a coarser microstructure, leading to increased porosity and crack formation [55]. Additionally, the high temperature accelerates water evaporation from the fresh compounds, hindering the reaction progress and further increasing porosity [56]. The average compressive strength of the acid-activated geopolymers, however, was only marginally higher than that of the HT group and significantly lower than that of the LT group.

The compressive strength of the LT group gradually decreased as the boric acid content increased. The observed decline was likely caused by a reduction in the pH of the alkali activator after the introduction of

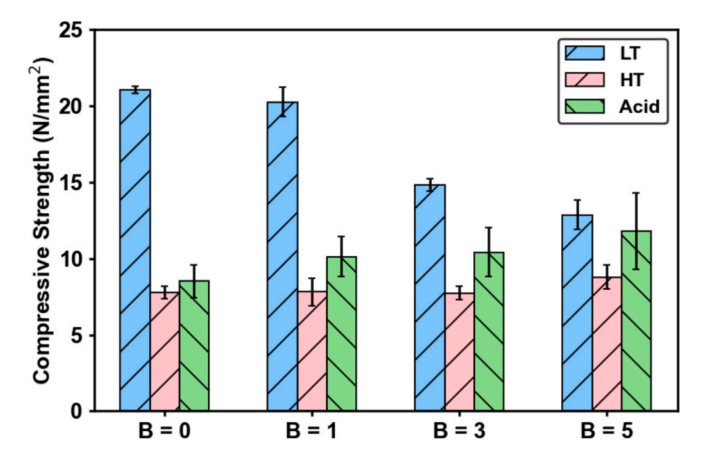


**Fig. 1.** Compressive strength of geopolymer samples after curing with varying B content.

boric acid (Table 2), which hindered the dissolution and reaction of metakaolin, thereby lowering the extent of geopolymerisation. Additionally, this may also be attributed to the increased number of negatively charged AlO<sub>4</sub> tetrahedra in alkali-activated geopolymers with a lower Si/(Al + B) ratio. As a result, more network modifiers (K<sup>+</sup> cations) are required to bind with oxygen atoms and form non-bridging oxygens, which reduce the connectivity of the network structure [57]. Moreover, a low Si/(Al + B) ratio reduces the proportion of Si tetrahedra and Si-O-Si units, which are essential for improving compressive strength [58]. In contrast, the compressive strength of the HT group was not significantly affected by the addition of boric acid. It is hypothesised that the stabilisation of the compressive strength in the HT group is primarily due to the internal voids and cracks, which are more significant determinants of compressive strength than the matrix itself, especially under hightemperature curing. Additionally, the elevated curing temperature likely enhanced the geopolymerisation process, mitigating the negative impact of boric acid incorporation on the geopolymer matrix's strength. In contrast to alkali-activated geopolymers, the samples from the acidactivated geopolymer group exhibited an increase in compressive strength with rising B content, consistent with previous studies [59]. While earlier research attributed the increase in compressive strength to the reaction between boric acid and phosphoric acid, which leads to the formation of an amorphous borophosphate secondary phase precipitating within the geopolymer framework (Eq. 4). However, this study identifies a different cause.

$$H_3PO_4 + H_3BO_3 \rightarrow BPO_4 + 3H_2O$$
 (4)

Fig. 2 illustrates the fracture surfaces of acid-activated geopolymers after compressive strength testing. The Acid-0 sample (Fig. 2 (a)) displayed numerous pores and voids that significantly reduced the density and compressive strength of the bulk material. These defects were believed to originate from the initial dealumination stage of geopolymerisation, which generated substantial heat, with the internal temperature of the samples reaching up to 120 °C [45]. Such high temperatures caused the water in the fresh mixture to boil, leading to the rapid evaporation of water and the formation of numerous pores and cracks. Conversely, introducing boric acid notably reduced the cracks and pores in the boron-containing geopolymer samples (Fig. 2 (b-d)),

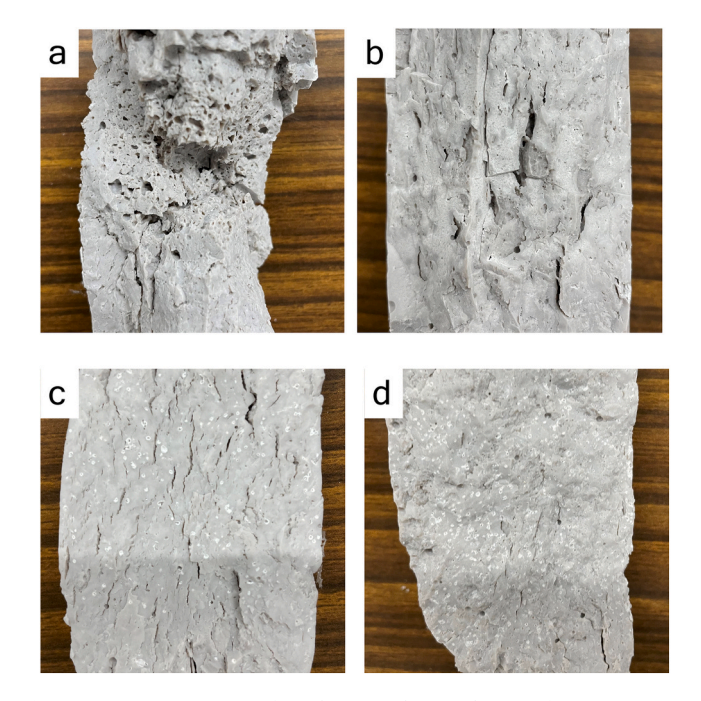


Fig. 2. Fracture sections of acid-activated geopolymer after compressive strength testing: (a) Acid-0, (b) Acid-1, (c) Acid-3, and (d) Acid-5.

resulting in an obvious increase in strength. This effect cannot be attributed to changes in the activation properties of the acid activator, as the addition of boric acid did not alter the pH of the acid activator (Table 2). The primary reason was likely due to the endothermic reaction between boric acid and phosphoric acid, which absorbed a significant amount of heat during the dealumination stage. This heat absorption lowered the internal temperature, reduced water loss and cavity formation, and lead to a denser geopolymer structure. In addition, as the amount of boric acid introduced increases, white spots can be observed in the samples, which may be the incompletely reacted portion of the boric acid (Fig. 2 (b-d)).

#### 3.2. Chemical characteristics of samples

#### 3.2.1. XRD

Fig. 3 presents the X-ray diffraction (XRD) patterns of the metakaolin precursor and the geopolymer samples after their respective curing processes. The XRD pattern of the metakaolin precursor displays a broad hump in the  $2\theta$  range of  $15{\text -}30^\circ$  (peaking around  $22^\circ$ ), accompanied by minor crystalline peaks of anatase (TiO<sub>2</sub>) and quartz (SiO<sub>2</sub>), which persist as inert phases in all the samples. Upon activation, the broad hump in all alkali-activated geopolymers shifts to  $20{\text -}35^\circ$  (peaking around  $29^\circ$ ), regardless of the curing conditions. In contrast, the broad hump in acid-activated geopolymers shifts to  $17{\text -}35^\circ$  (peaking around  $26^\circ$ ). This suggests that alkali-activated geopolymers have relatively

Diffraction angle, 2θ (°)

shorter interatomic distances compared to acid-activated ones, which exhibit a more disordered short-range structure. Notably, the introduction and varying content of boron did not visibly affect the crystal structure of the geopolymers in any group, nor did it introduce new characteristic peaks due to boric acid incorporation.

# 3.2.2. <sup>11</sup>B MAS NMR

Fig. 4 presents the <sup>11</sup>B MAS NMR spectra for all samples with boron incorporation, alongside spectra for boric acid (the boron source) and potassium tetraborate (used as a reference). The predominant peaks in boric acid appeared at  $\delta=10$  and 16 ppm, corresponding to ring 3-coordinated B and non-ring 3-coordinated B in  $BO_3$ , respectively [60]. In potassium tetraborate, in addition to the two types of BO<sub>3</sub>, BO<sub>4</sub> (4B, OSi) units were also present, with NMR resonances observed around  $\delta=2$ ppm [61]. Upon introducing boric acid into the LT group geopolymer samples, the concentration of both types of BO<sub>3</sub> units decreased, while a new resonance appeared around  $\delta = 1$  ppm (Fig. 4 (a)). This resonance arises from the convolution of BO<sub>4</sub> (xB, 4-xSi) units near  $\delta = 0$  ppm, representing the Si-bonded BO<sub>4</sub> (xB, 4-xSi) units, and the Si-unbonded  $BO_4$  (4B, 0Si) units at  $\delta = 2$  ppm, similar to the B in potassium tetraborate (Fig. 4 (d)). This observation suggests that adding boric acid to potassium-based alkali-activated geopolymers with low-temperature curing leads to the formation of potassium tetraborate, where some BO3 units from the boric acid are converted into BO4 units, with a portion of these BO<sub>4</sub> units connecting to Si within the geopolymer

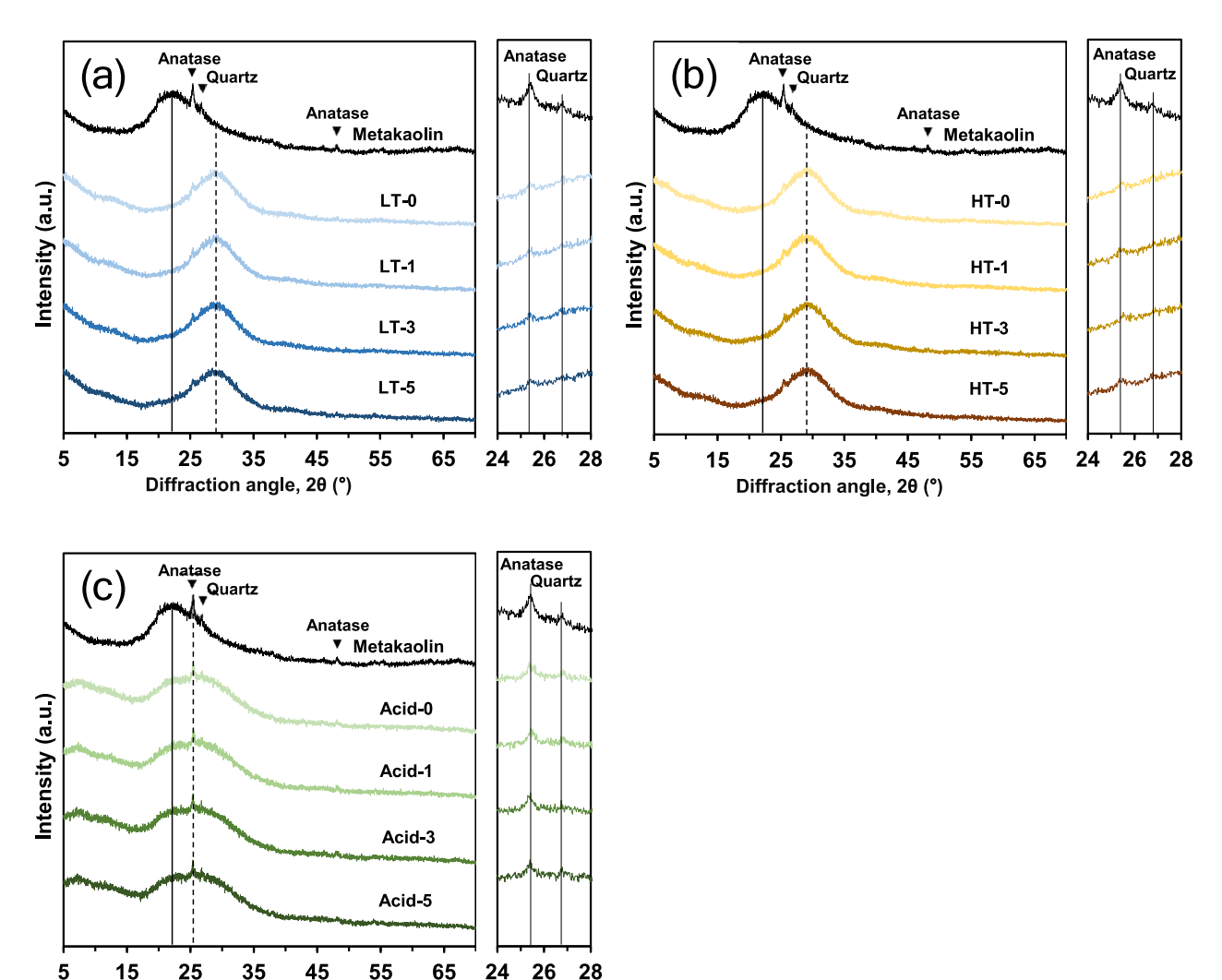


Fig. 3. X-ray diffraction (XRD) patterns of metakaolin and geopolymer samples: (a) LT group, (b) HT group and (c) Acid group.

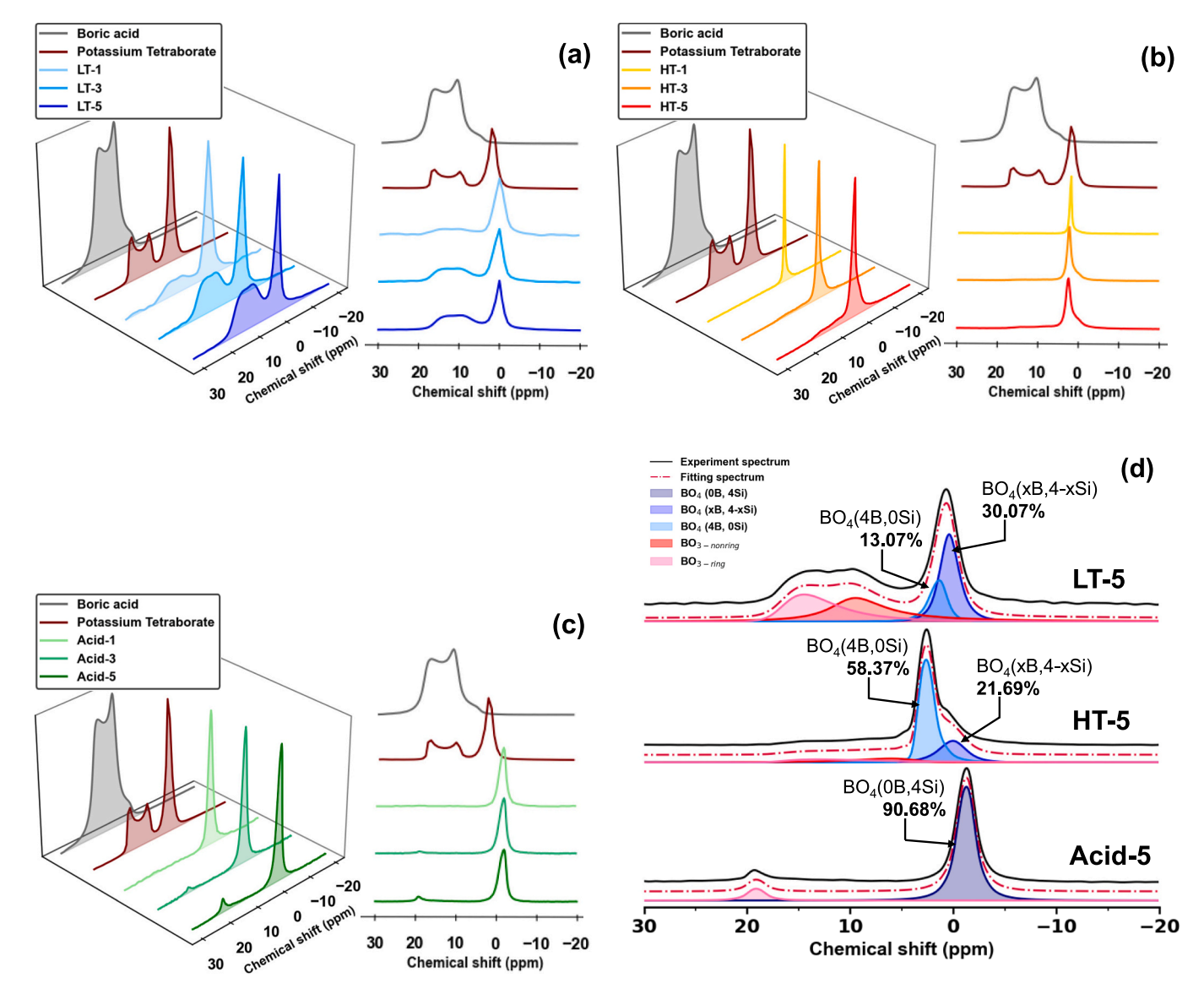


Fig. 4. <sup>11</sup>B MAS NMR spectra of boric acid, potassium tetraborate, and all geopolymer samples (normalised to the maximum spectral intensity): (a) LT group, (b) HT group, (c) Acid group, and (d) Deconvolution results for samples with the highest content of B in the three group types of geopolymers.

framework. Furthermore, the residual content of the two unconverted  ${\rm BO}_3$  compounds in the LT group samples increased proportionally with the amount of boric acid added.

After high-temperature curing, the HT group showed a similar proportional increase in  $BO_3$  units with the increase of boric acid addition, though this increase was significantly less pronounced compared to the LT group. The primary peak corresponding to the  $BO_4$  unit shifted towards the low-field direction and exhibited clear asymmetry. Deconvolution results revealed that this asymmetry is primarily due to an increase in Si-unbonded  $BO_4$  (4B, 0Si) units, while the proportion of Si-bonded  $BO_4$  (xB, 4-xSi) units decreased, particularly in the high boron content samples at 5 wt% (Fig. 4 (d)). These observations suggest that high-temperature curing facilitates the conversion of  $BO_3$  units from boric acid to  $BO_4$  units. However, the formation of Si-bonded  $BO_4$  (xB, 4-xSi) units may not necessarily increase, possibly due to the specific properties of the geopolymer matrix under varying temperature conditions

In the acid-activated geopolymer samples (Fig. 4 (c)), the non-ring BO $_3$  units introduced by boric acid nearly disappeared, while the ring BO $_3$  units remained. Additionally, a symmetric peak emerged at  $\delta = -1.5$  ppm, corresponding to BO $_4$  units fully coordinated with four Si

atoms, which results in a shift towards the high-field region due to increased electromagnetic shielding [60]. Although the amount of residual ring BO $_3$  increases slightly with the increase of boric acid, the dominant form of B is BO $_4$ , with over 90% of the BO $_4$  (0B, 4Si) units formed in samples containing 5 wt% boric acid (Fig. 4 (d)). This indicates that boric acid predominantly converts non-ring BO $_3$  into BO $_4$  units upon incorporation into acid-activated geopolymers and tends to bond with Si until saturation. Furthermore, it is noteworthy that no signal was detected around  $\delta = -4.1$  ppm, where a resonance attributed to the BO $_4$  from BPO $_4$  is expected [62], suggesting that the second phase of BPO $_4$  may not be present in the final acid-activated geopolymer matrix.

# 3.2.3. <sup>27</sup>Al MAS NMR

In most porous aluminosilicate solids,  $^{27}$ Al nuclei typically exhibits 4-, 5-, and 6-fold coordination structures, with chemical shifts ranging from low to high field [63]. Fig. 5 (a) shows the  $^{27}$ Al MAS NMR spectrum of metakaolin, which serves as an aluminosilicate precursor for all groups of geopolymer, along with its deconvolution results. As in other aluminosilicate solids, the  $^{27}$ Al nuclei in metakaolin is present as Al<sub>4</sub>, Al<sub>5</sub> and Al<sub>6</sub>, all of which display distinct NMR resonances. Upon the alkali

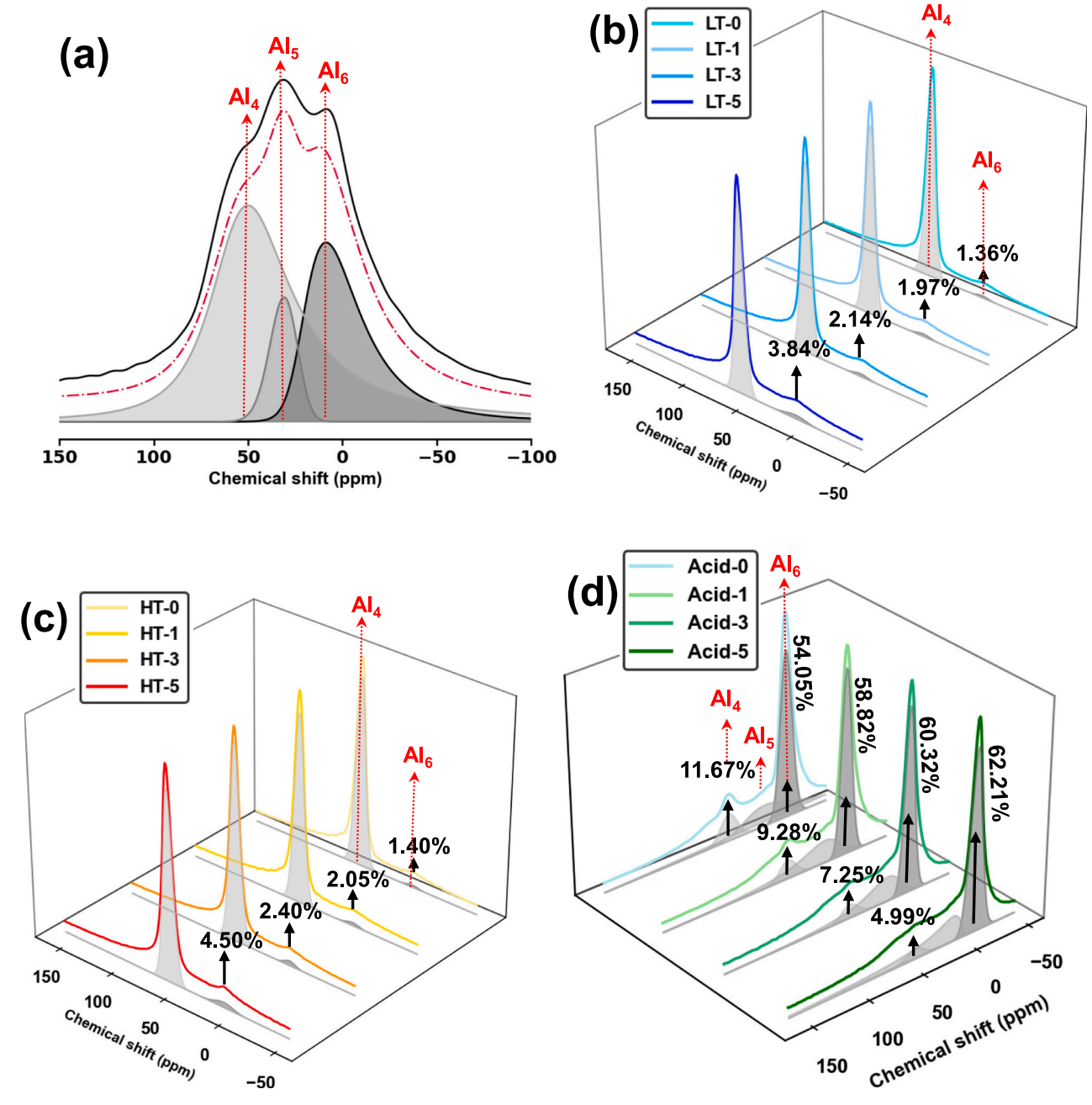


Fig. 5. <sup>27</sup>Al MAS NMR spectra (normalised to the maximum spectral intensity) and molar proportions of Al structural units derived from spectral deconvolutions for (a) Metakaolin, (b) LT group, (c) HT group, (d) Acid group.

activation (Fig. 5 (b) and (c)), the  ${\rm Al}_5$  and  ${\rm Al}_6$  units were transformed into  ${\rm Al}_4$  units, with the  ${\rm Al}_5$  unit disappearing entirely and the  ${\rm Al}_6$  unit nearly disappearing. Since  ${\rm Al}_6$  originates from the metakaolin precursor and converts to  ${\rm Al}_4$  following alkali activation, the remaining amount of  ${\rm Al}_6$  can indicate the extent of the initial depolymerisation phase in geopolymerisation. The content of  ${\rm Al}_6$  in the geopolymer samples increased progressively with higher amounts of added boric acid, which suggests that the degree of depolymerisation of metakaolin in the alkali activation solution decreased with the addition of boric acid. This result is likely due to the impact of boric acid on the pH of the alkali activation solution and aligns with the observed compressive strength (Fig. 1). The  ${\rm Al}_6$  content in the samples of HT group at all boric acid contents was slightly higher than in the LT group, suggesting that high-temperature curing has a relatively adverse effect on the initial depolymerisation phase of geopolymerisation compared to low-temperature curing. This is

because, although high temperatures can promote geopolymerisation, they also cause rapid water evaporation, reducing the continuous phase within the system. This significantly shortens the duration of the initial depolymerisation stage, leading to insufficient dissolution of Al $_6$  units in the metakaolin precursor. Nonetheless, the difference in Al $_6$  content between the HT and LT groups was  $<\!1\%$  for samples with all boric acid contents, indicating that the negative impact of high-temperature curing on alkali-activated geopolymers was minimal.

Fig. 5 (d) presents the  $^{27}$ Al MAS NMR spectra and deconvolution results for the acid group samples. The spectra are mainly composed of Al in 4-, 5-, and 6-coordination. Compared to the Al units in metakaolin, the chemical shifts of Al<sub>4</sub> remained unchanged, whereas those in 5- and 6-coordination shifted to higher fields. A previous study [48] has demonstrated that, unlike alkali activation, acid activation consumed all types of Al units during the initial dealumination phase of

geopolymerisation. Subsequently, new 5- and 6-coordination Al structures were predominantly formed and linked to -OP and -OSi groups. Since P has stronger electronegativity than O and Si, the NMR chemical shift of the newly generated Al-OP structures is closer to the high-field range than that of Al-OSi or Al-OH. In contrast, the 4-coordination Al structure in geopolymers primarily originated from partially unreacted Al<sub>4</sub>-SiO or Al<sub>4</sub>-OH units in the metakaolin precursor due to its relatively more stable structure compared to the other two coordinated Al configurations. The deconvolution results indicate that the amount of unreacted Al<sub>4</sub> units in the geopolymer decreased progressively with increased addition of boric acid, while the proportion of Al<sub>6</sub> units

increased. This suggests that the introduction of boric acid facilitated the dealumination process, leading to the conversion of more  $\mathrm{Al}_4$  units in the metakaolin precursor into  $\mathrm{Al}_6$  structures. This effect is likely due to the capacity of boric acid to absorb significant reaction heat through its endothermic reaction with phosphoric acid during the early dealumination stage. This process can mitigate rapid water evaporation, thereby promoting acid-activated geopolymerisation, which aligns with the observed increase in compressive strength (Fig. 2).

# 3.2.4. <sup>29</sup>Si MAS NMR

In general, the chemical environment of Si in aluminosilicate

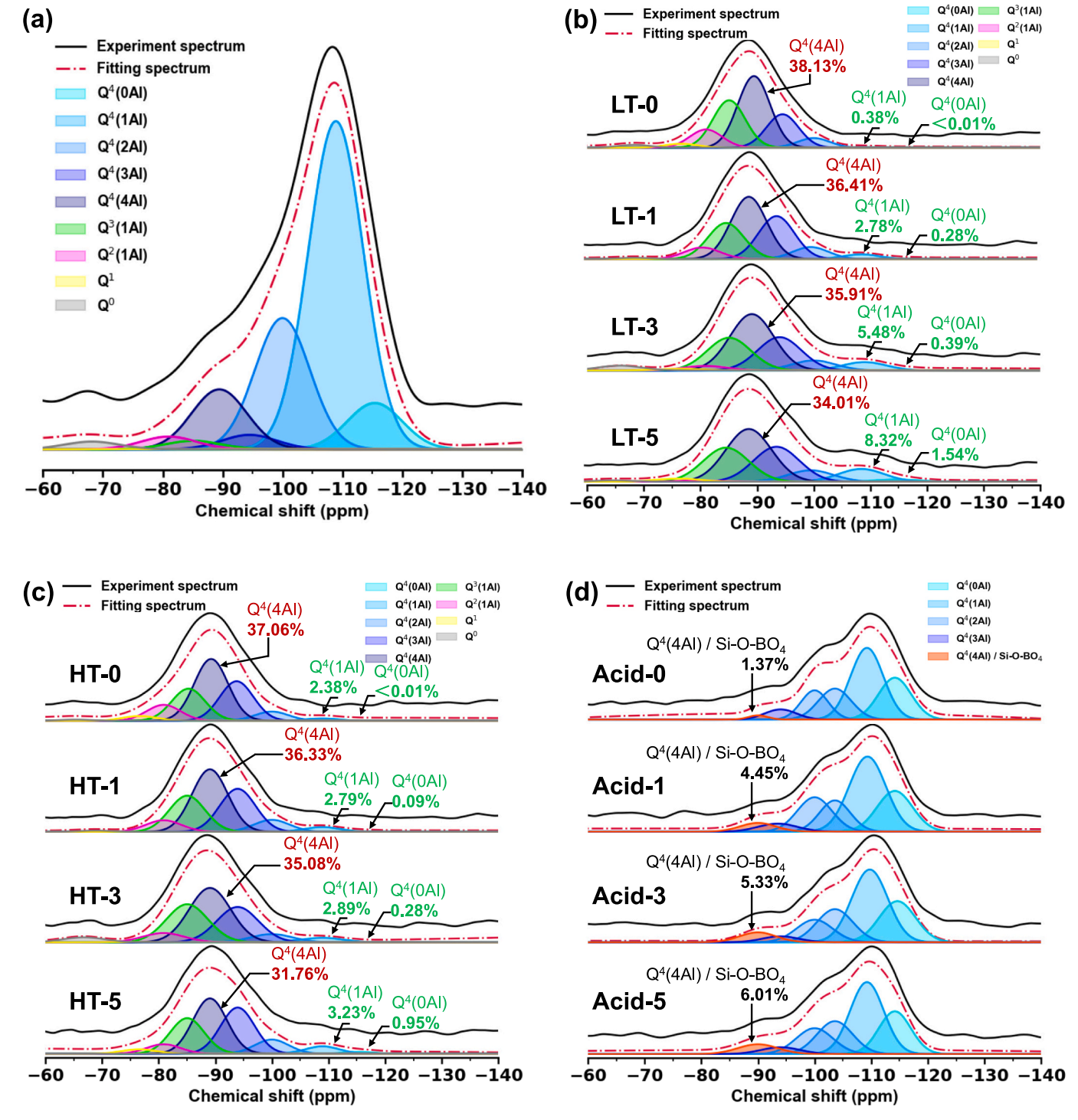


Fig. 6. Deconvolution results of <sup>29</sup>Si MAS NMR spectra and molar proportions of Si structural units for (a) Metakaolin, (b) LT group, (c) HT group and (d) Acid group.

materials, represented as  $Q^n(mAl)$ , is characterised by the number of tetrahedral atoms (n) surrounding the Si tetrahedron and the number of bonded Al atoms (m). Previous studies have identified various Si environments in geopolymers, including  $Q^0,\,Q^1,\,Q^2(1Al),\,Q^3(1Al),\,Q^4(4Al),\,Q^4(3Al),\,Q^4(2Al),\,Q^4(1Al)$  and  $Q^4(0Al),$  with corresponding chemical shifts of approximately  $\delta=-68\pm5,\,-76\pm5,\,-80\pm3,\,-86\pm4,\,-88\pm3,\,-94\pm4,\,-100\pm5,\,-105\pm4,\, and\,-115\pm4$  ppm, respectively [45,48]. Fig. 6 (a) presents the  $^{29}$ Si MAS NMR spectrum of metakaolin, an aluminosilicate precursor for all geopolymer groups, along with its deconvolution results. The primary structure of Si in metakaolin consisted of Al-unsaturated Si tetrahedra (Q^4(mAl)), with over 85% of m not exceeding 2. Additionally, the content of non-tetrahedral Si species (Q^n, where n<4) was <5%.

Fig. 6 (b) and (c) show the <sup>29</sup>Si MAS NMR patterns of the alkaliactivated geopolymer samples from the LT and HT groups, respectively, along with the deconvolution results. The deconvolution results indicate a significant reduction in Al-unsaturated Si tetrahedra in metakaolin upon alkali activation, accompanied by an increase in nontetrahedral Si content. This suggests that the Si structure in the metakaolin precursor underwent depolymerisation, producing a substantial amount of free Si, and a large amount of Al then bonds with the structure during the subsequent polymerisation process. However, the geopolymers in the HT group contained slightly fewer Q<sup>4</sup>(4Al) units and a higher proportion of low-aluminium Si tetrahedral units compared to the LT group. This is because high curing-temperature accelerated water evaporation during the initial depolymerisation phase, leading to fewer free Al units available in the matrix for subsequent polycondensation (Fig. 5 (a) and (b)). With increasing boric acid content, the  $Q^4(4Al)$  units in both LT and HT samples decreased, while the low-aluminium Si tetrahedral units correspondingly increased. The HT samples exhibited a more substantial decrease in Q<sup>4</sup>(4Al) units, whereas the LT samples showed a more pronounced increase in the low-aluminium Si tetrahedral units. Since B can replace Al in borosilicate aluminates and bond with Si to form Si-O-B structures [64], the Q<sup>4</sup>(4Al) units decreased as the B content increased. The relatively higher reduction of Q<sup>4</sup>(4Al) units in the HT samples suggests that elevated curing temperature facilitated the substitution of B for Al. The decrease in the signal intensity for the lowaluminium Si tetrahedral units can be attributed to a reduction in geopolymerisation caused by adding boric acid, which increased the formation of unsaturated Si tetrahedra. In addition, the more pronounced signal increase in the LT group indicates that geopolymerisation is significantly impeded by boric acid in the LT group samples. In contrast, the HT samples appeared less affected due to the high-temperature curing, which partially mitigated the boric acid's negative impact on geopolymerisation. This observation aligns with the compressive strength results shown in Fig. 1.

Fig. 6 (d) presents the <sup>29</sup>Si NMR spectra of the acid group samples, along with their deconvolution results. In contrast to the alkali-activated geopolymers in the LT and HT groups, the <sup>29</sup>Si MAS NMR resonances of the acid-activated geopolymers were predominantly located within the chemical shift range characteristic of tetrahedral Si, suggesting that acid activation has largely dealuminated the Al in the metakaolin precursor with little destruction of the original Si-O-Si bonds. Compared to alkaliactivated geopolymers, the tetrahedral Si in acid-activated geopolymers remained mostly unsaturated, with a significant presence of Si-O-Si bonds. The most notable change in the signals of the acid-activated samples after adding boric acid was observed at a chemical shift of approximately  $\delta = -90$  ppm, where the intensity increased with the introduction of boric acid. These signals at around  $\delta = -90$  ppm correspond not only to the saturated tetrahedral Si Q<sup>4</sup>(4Al) structures but are also attributed to Si-O-BO<sub>4</sub> structures, as reported in a previous study [65]. The <sup>27</sup>Al MAS NMR results indicate that introducing boric acid leads to an increase in 6-coordinated Al within the geopolymers. In contrast, a previous study demonstrated that the amount of Q<sup>4</sup>(4Al) units in acid-activated geopolymers is inversely proportional to the amount of Al<sup>6</sup> produced [48]. Consequently, the resonance signals associated with Q<sup>4</sup>(4Al) were expected to decrease as more boric acid was added. However, in this case, the signal eventually increased with higher B content. This increase was attributed to the intensified NMR signal corresponding to Si-O-BO<sub>4</sub> structures, which outweighed the decrease in the Q<sup>4</sup>(4Al) unit signal. These findings suggest that the primary factor driving the signal increase at  $\delta = -90$  ppm with higher B content is the conversion of BO<sub>3</sub> in boric acid to BO<sub>4</sub> and its subsequent incorporation into the Si network, leading to the formation of Si-O-BO<sub>4</sub> structures.

Notably, although the  $^{11}B$  MAS NMR results indicate the formation of Si-O-BO<sub>4</sub> bonds in both the LT and HT groups, the  $^{29}Si$  MAS NMR spectra (Fig. 6 (b) and (c)) show no observable increase in signal intensity around the  $\delta=-90$  ppm chemical shift with increasing B content. This absence of signal increase may be due to the overlap of the Si-O-BO<sub>4</sub> signal with the Q<sup>4</sup>(4Al) signal, where the decrease in Q<sup>4</sup>(4Al) signal intensity is more pronounced than any potential increase in the Si-O-BO<sub>4</sub> signal.

#### 3.2.5. <sup>31</sup>P MAS NMR

The geopolymer in the acid group contains a significant amount of P, attributed to the reaction of the phosphoric acid activator with metakaolin. In fully geopolymerised samples, P predominantly appears in two forms: the far-Si terminal P (-Si-O-Al<sub>4/5</sub>-O-P-) and the near-Si terminal P (-Si-O-P-O-Al<sub>4/5/6</sub>-) [48]. Fig. 7 shows the  $^{31}P$  MAS NMR spectra for the acid group samples. All spectra display broad signals between  $\delta=0$  and -30 ppm, corresponding to the  $^{31}P$  MAS NMR signals in the samples. Due to the disordered structure of the geopolymers, distinguishing between the two types of P is challenging. However, the near-Si terminal P appeared in a relatively higher-field region compared to the far-Si terminal P due to the greater electronegativity of Si. While the signal profiles show no major variation with differing B content, a

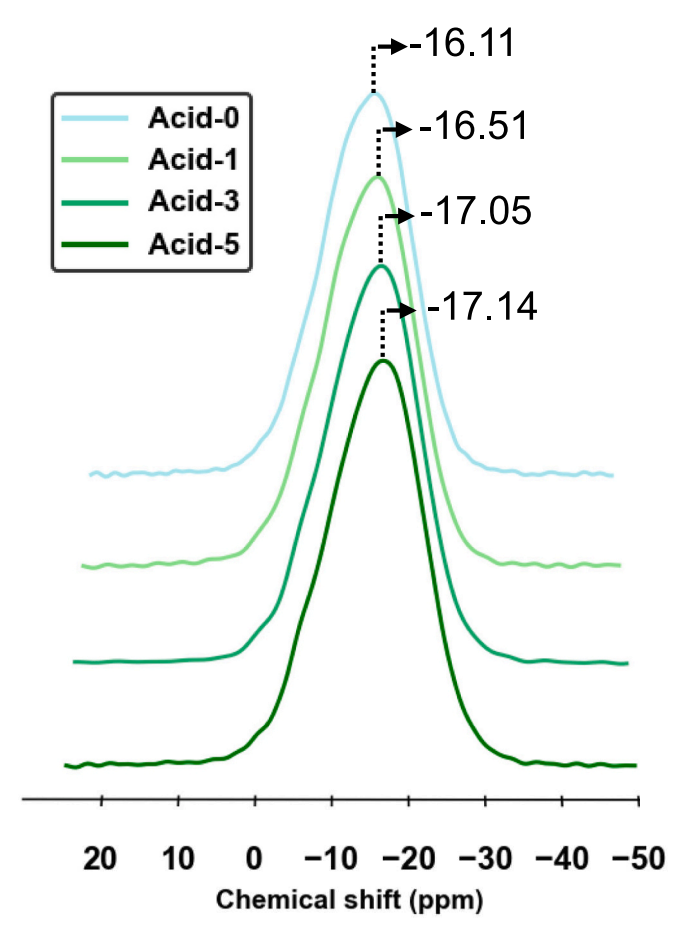


Fig. 7. <sup>31</sup>P MAS NMR spectra for acid group samples.

noticeable shift towards the high-field region with increasing B was observed. This suggests that while boric acid had minimal impact on the overall P chemical environment in acid-activated geopolymers, it may increase the proportion of near-Si terminal P, which is positively correlated with the Al<sub>6</sub> content [48]. This correlation may partially explain the increase in Al<sub>6</sub> observed in the <sup>27</sup>Al MAS NMR results with higher B content. Furthermore, it is notable that the <sup>31</sup>P MAS NMR spectra display none of the expected resonance signals associated with products from the reaction between boric acid and phosphoric acid, such as the BPO4 signal typically observed in borophosphate glasses around  $\boldsymbol{\delta}$ = -30 ppm [66], nor the -B-P-B- signal at approximately  $\delta = -6$  ppm in the borax-wasteform solidified by phosphoric acid-based geopolymers [59,67]. This indicates that while the reaction between boric acid and phosphoric acid (Eq. 4) occurred during the early stages of geopolymerisation, absorbing substantial reaction heat to form BPO<sub>4</sub> or -B-P-B- structures, these structures were subsequently degraded into the geopolymer matrix as geopolymerisation progressed. Consequently, the hypothesis that a B-related secondary phase contributed to compressive strength is unsupported (Fig. 1).

#### 3.3. Micromorphology characteristics

Fig. 8 presents scanning electron micrographs of the geopolymer samples. Although the compressive strength and NMR results suggest that the HT samples may have higher porosity and a looser matrix structure compared to the LT samples, no significant difference was observed in the corresponding SEM images (Fig. 8a and b). This may be due to the difficulty in detecting larger macro pores (>10  $\mu$ m), which have a greater impact on compressive strength at this magnification level [68]. Nevertheless, aggregation of small particles, likely unreacted metakaolin, was evident in all alkali-activated geopolymers (Fig. 8 (a)

and **(b)**). A significant increase in unreacted metakaolin was observed with rising B content in the LT group, while this increase was less pronounced in the HT group. In contrast, geopolymers with low B content in the acid group showed pronounced cracks with whitish edges, likely caused by rapid water evaporation due to intense reaction heat during geopolymerisation (Fig. 8 **(c)**). However, geopolymers in the acid group exhibited smoother gel connectivity with increasing B content, suggesting that adding boric acid enhanced the acid-activated geopolymerisation process.

#### 3.4. Chemical bonding information of samples

Fig. 9 presents the FTIR data for all groups of geopolymers. As evidenced by prior studies [69,70], the primary signals in alkali-activated geopolymers are as follows: the band at 1515-1645 cm<sup>-1</sup> corresponded to -OH bond; the broad band centred at 1406 cm<sup>-1</sup> was attributed to ambient CO2; asymmetric and symmetric vibrational signals of T-O-T (T = Si or Al) were found within the broad band at 900-1200 cm<sup>-1</sup> and at 680 cm<sup>-1</sup>, respectively; and the peaks at 860, 570, and 450 cm<sup>-1</sup> corresponded to Si-O/OH stretching and bending, as well as symmetric stretching of Al-O and Si-O. In contrast, for acidactivated geopolymers, the key signals are described as follows [71–73]: the signals at 1210 and 1140  $cm^{-1}$  corresponded to P=O vibrations; signals at 900 and 630 cm<sup>-1</sup> were from Si-O-P and O-P-O vibrations, respectively; asymmetric and symmetric T-O-T (T = Si or Al) structures were observed in the broad band at 900-1200 cm<sup>-1</sup> and at 720 cm<sup>-1</sup>; while symmetric Si-O-Si and other Si-O vibrations occurred at 795 cm<sup>-1</sup> and approximately 450 cm<sup>-1</sup>.

Two distinct signals were observed to progressively intensify with increasing B content in the LT group (Fig. 9 (a)). The signals corresponded to the O-B-O vibration at  $450~\text{cm}^{-1}$ , linked to the ring BO<sub>3</sub>

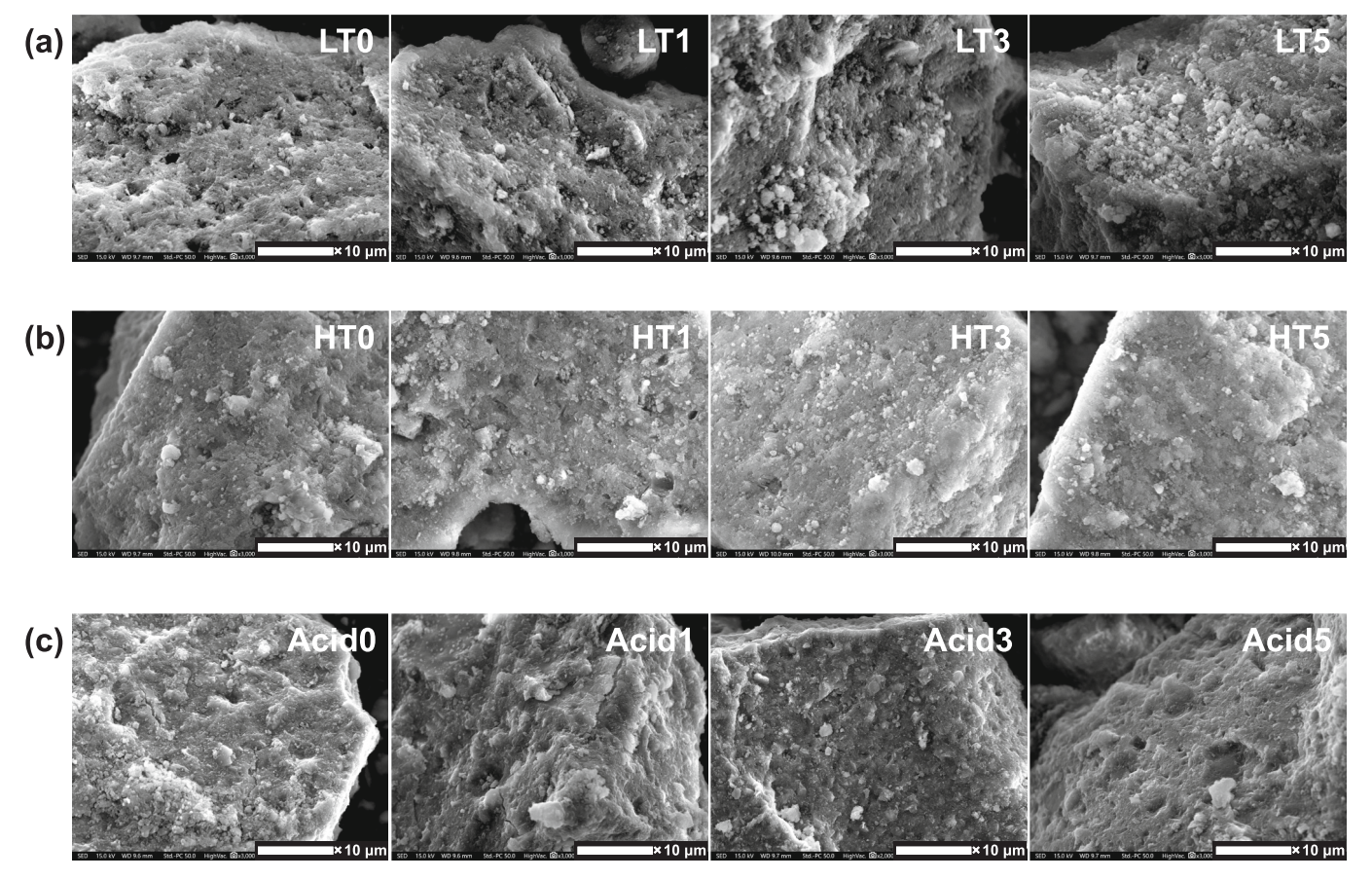


Fig. 8. SEM micrographs of (a) LT group, (b) HT group, and (c) Acid group samples.

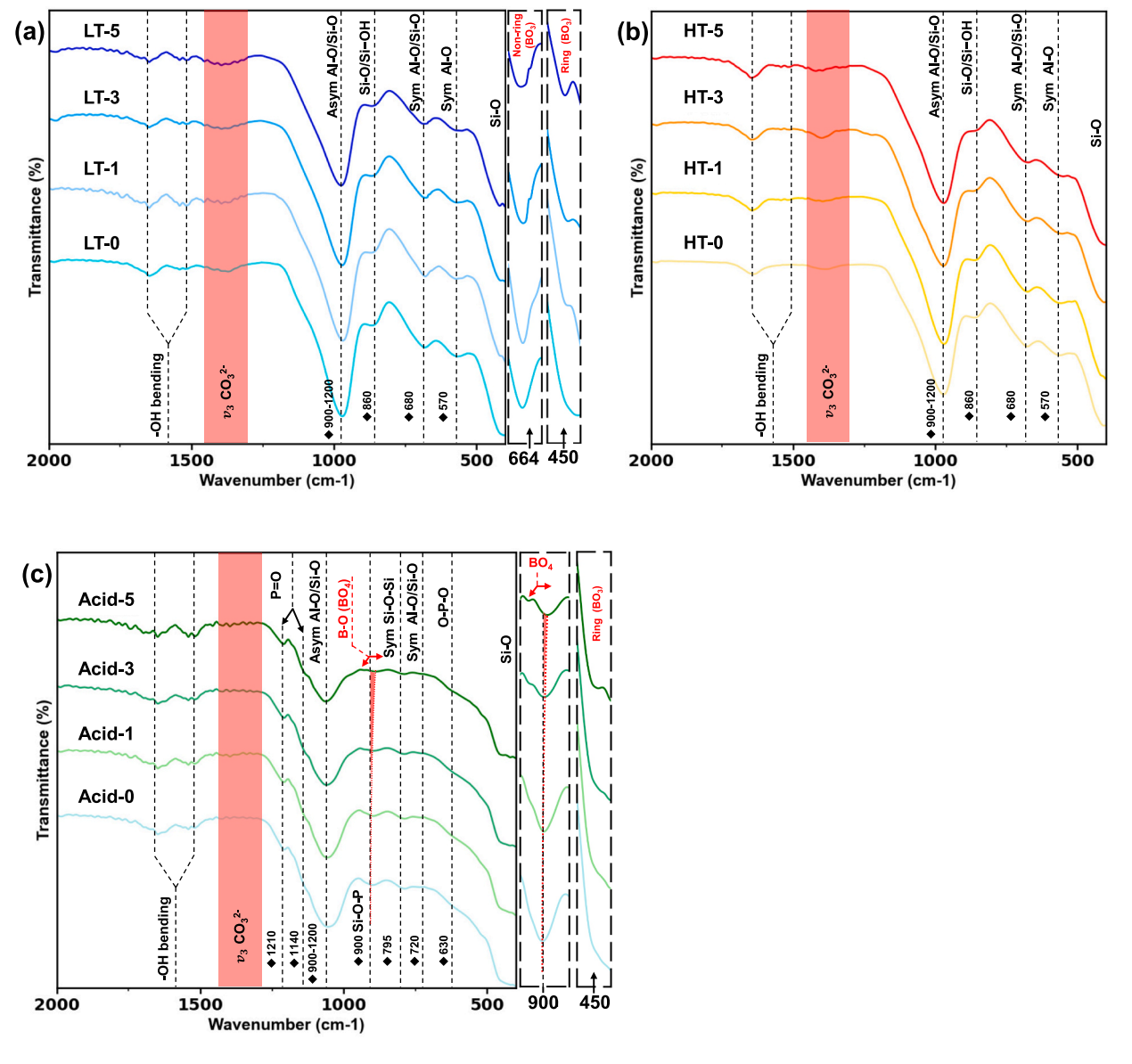


Fig. 9. FTIR spectra of (a) LT group, (b) HT group, and (c) Acid group samples.

structure, and the out-of-plane bending of the B—O vibration at 664 cm $^{-1}$ , associated with the non-ring BO<sub>3</sub> structure [74]. This result was not observed in the HT group (Fig. 9 (b)), suggesting that the conversion of BO<sub>3</sub> to BO<sub>4</sub> was nearly complete in alkali-activated geopolymers under high temperature, consistent with the  $^{11}$ B MAS NMR findings. However, no vibration signals attributed to BO<sub>4</sub> were detected, likely because the asymmetric BO<sub>4</sub> vibrations, typically occurring around  $1060-1130~\text{cm}^{-1}$  [74], may be obscured by the dominant peaks of the geopolymer matrix between 900 and  $1200~\text{cm}^{-1}$ .

Two signals that varied obviously with increasing B content were also observed in the acid group samples (Fig. 9 (c)). One was a vibration signal at 450 cm<sup>-1</sup>, attributed to the ring BO<sub>3</sub>, similar to the LT group, indicating that non-ring BO<sub>3</sub> was the primary component consumed upon the addition of boric acid to the acid-activated geopolymer. The other signal, around 900 cm<sup>-1</sup>, can be resolved into two peaks: one shifted to the right of the peak originally assigned to Si–O–P, while the other occurred at approximately 928 cm<sup>-1</sup>. Signals in this region were attributed to symmetric BO<sub>4</sub> vibrations [74,75], suggesting that BO<sub>4</sub> in acid-activated geopolymers differs from the asymmetric BO<sub>4</sub> (xB, 4-xSi) observed in the LT and HT groups, existing primarily as symmetric BO<sub>4</sub>

(0B, 4Si). These findings are consistent with the <sup>11</sup>B MAS NMR analysis.

# 3.5. Stability in aqueous environments

Radioactive debris solidified in the geopolymer matrix will ultimately be disposed of in geological repositories. The stability of geopolymers in aqueous environments, such as near-surface groundwater, requires rigorous evaluation. Fig. 10 presents the leaching results of three sample groups in a laboratory-simulated aqueous environment, including the structural elements Si and Al, as well as B, which is introduced as the neutron absorber. The leaching behaviour of B is shown in Fig. 10 (a). In the LT group (Fig. 10 (a -1 and -4)), B exhibited significant leaching during both static and dynamic tests, with the final equilibrium leaching fraction exceeding 98% in both cases. However, the rate of increase was slightly lower for static leaching during the initial and middle stages compared to dynamic leaching. This indicates that B in alkali-activated geopolymers cured at low temperatures failed to form a stable chemical bond with the geopolymer matrix and was thus not fully integrated into it. In the HT group (Fig. 10 (a -2and -5)), a slight reduction in B leaching was observed compared to the

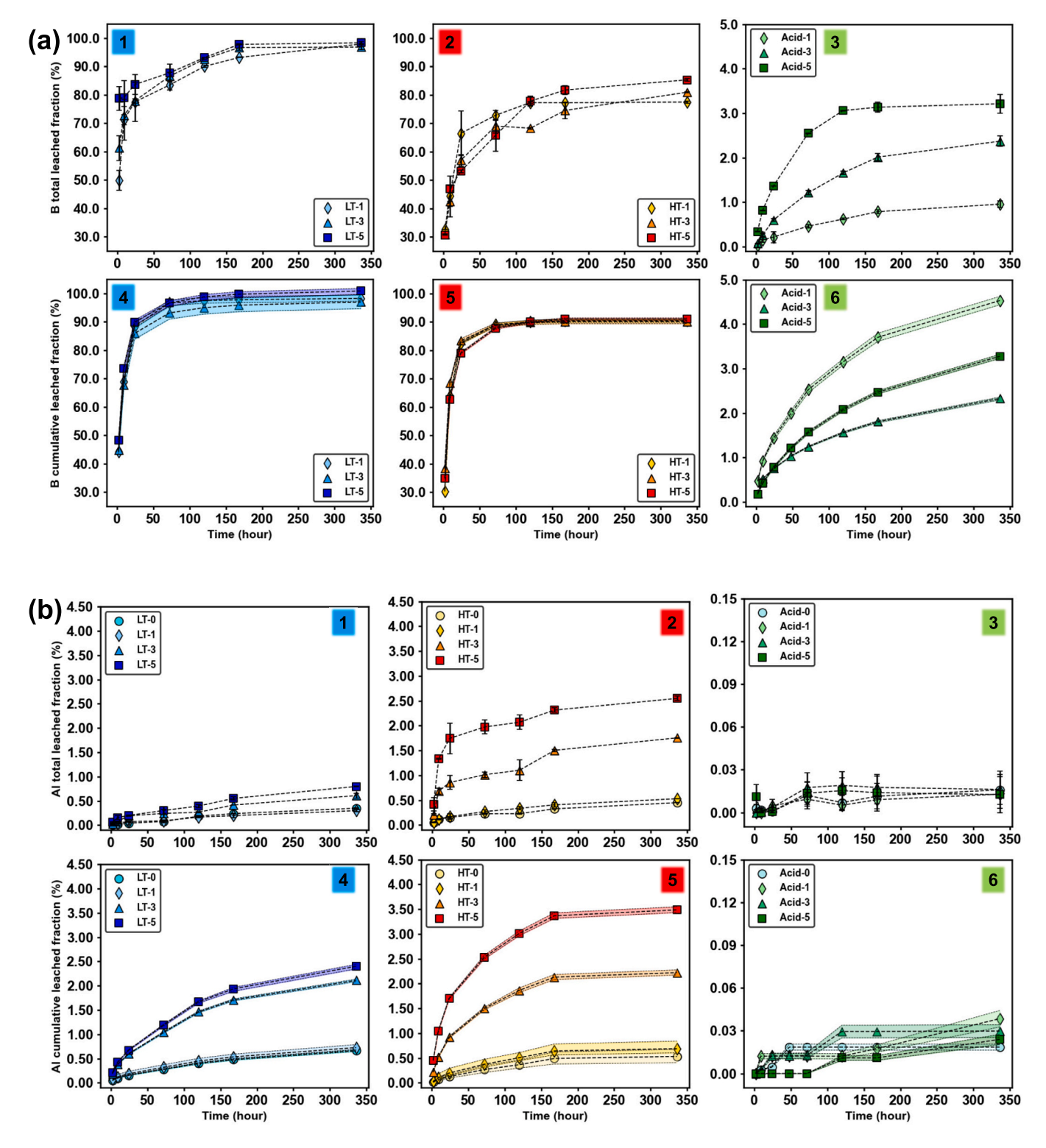


Fig. 10. Total leaching fractions (-4, -5, -6) for dynamic leaching test of (a) B, (b) Al, and (c) Si in all samples, with colour bands indicating confidence intervals.

LT group, with significantly lower leaching under the static condition than dynamic condition. This indicates that while high-temperature curing may enhance the incorporation of B into the geopolymer matrix to a certain extent, the structural instability or insufficient integration into the main matrix may lead to an increase in leached fraction to approximately 90% during the more aggressive dynamic leaching

process. In the acid group (Fig. 10 (a -3 and -6)), a substantial reduction in B leaching was observed. Equilibrium in static leaching was achieved after approximately 150 h, and although equilibrium in dynamic leaching had not been reached after 336 h, the increase had gradually started to level off. This suggests that B can be efficiently incorporated into the framework of the acid-activated geopolymer

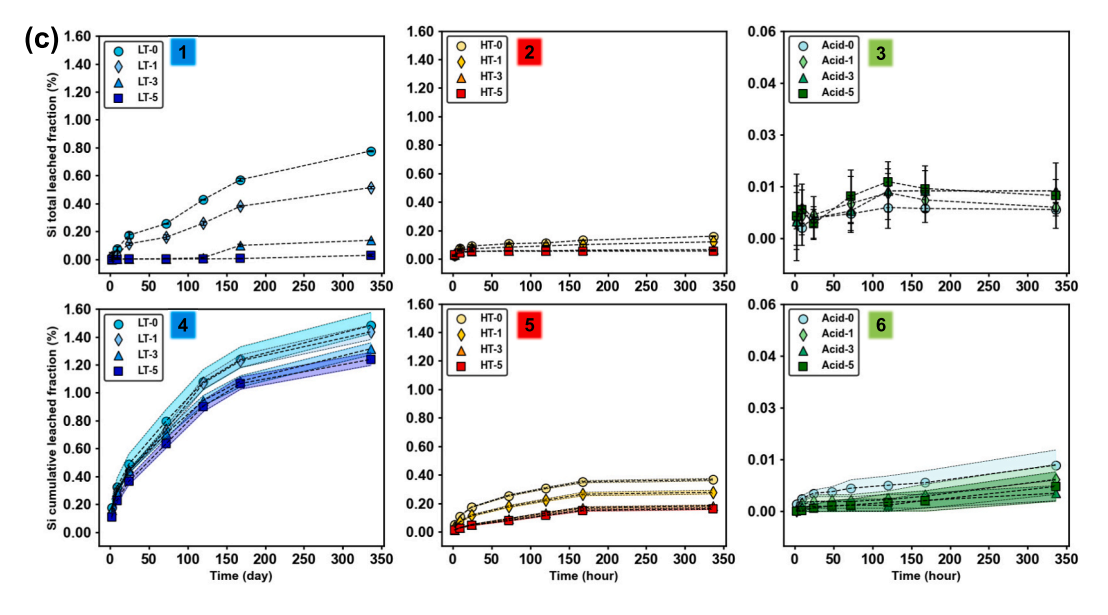


Fig. 10. (continued).

matrix. Interestingly, unlike the alkali-activated geopolymers, where the final leaching rate increased with B content in both static and dynamic leaching tests, the acid group showed that samples with the lowest B content (Acid-1) exhibited the highest leaching rates in the dynamic leaching tests. This is attributed to the fact that, in acid-activated geopolymers with low B content, through B can form stable chemical bonds with the matrix to some extent, the matrix may exhibit inherent structural defects due to incomplete geopolymerisation and the looser structure (Figs. 2, 5 and 8). These defects include short-range structures that were not fully incorporated into the matrix. Consequently, B associated with these less stable structures leaches out from the relatively loose matrix during the more aggressive dynamic leaching process than static.

Fig. 10 (b) presents the leaching results for Al. All alkali-activated geopolymer samples with low B content (0 and 1%) exhibited similar levels of Al leaching in both leaching processes (Fig. 10 (b - 1, -2, -4, -5)). This suggests that the amount of extra-framework aluminium (EFAL) was approximately the same. However, a further increase in B content led to a corresponding rise in Al leaching, more pronounced in the HT group than in the LT group. This could be attributed to the hindrance of geopolymerisation by boric acid and the competition between B and Al, increasing the amount of EFAL. In contrast, in the acid group (Fig. 10 (b - 3 and -6)), Al leaching was negligible under both leaching conditions, indicating that in acid-activated geopolymers, Al is almost fully incorporated into the matrix structure, regardless of B content.

A notable difference between the LT and HT groups is observed in the Si leaching results (Fig. 10 (c)). It is widely accepted that the leached Si consists of free Si units, which have undergone geopolymerisation but are not incorporated into the matrix structure [76]. During static leaching, the LT group exhibited higher Si leaching levels than the HT group in samples with low B content, with the difference diminishing as B content increased (Fig. 10 (c -1 and -2)). This may be because free Si units are partially bonded to BO<sub>4</sub> units, allowing them to remain within the structural framework during static leaching. However, in dynamic leaching, the LT group exhibited significantly higher Si leaching levels than the HT group, even in samples with high B content (Fig. 10 (c -4and - 5)). This is because geopolymerisation under low-temperature curing conditions is less efficient compared to higher temperatures (Fig. 6), resulting in a higher number of free Si units. These free Si units, when combined with BO<sub>4</sub> units, form short-range silicate structures that remain poorly integrated into the primary framework of the geopolymer

matrix. As a result, under dynamic and aggressive leaching conditions, these unstable structures are more prone to leaching. Nevertheless, the addition of B reduced Si leaching to some extent in both the LT and HT groups, suggesting that free Si partially bonded to BO<sub>4</sub> achieved some stabilisation within the structure compared to its state before bonding. However, this stability may be unreliable over time or under varying environmental conditions. It is also noteworthy that Al leaching was not lower in the HT group than in the LT group in all the cases, suggesting that the reduced Si leaching in the HT group is due to the more formation of low-aluminium structures with Si-O-Si bonds. This finding aligns with the <sup>29</sup>Si MAS NMR results and corresponds to the observed compressive strengths (Fig. 1). The Si leaching results for the acid group were similar to those for Al (Fig. 10 (b - 3 and - 6)), showing negligible leaching in both tests. This is partly attributed to the difficulty of dissolving Si from metakaolin using acid activators, which limits the formation of a short-range structure [45] and partly indicates that adding boric acid has a minimal negative impact on the matrix structure.

# 3.6. Mechanisms for the incorporation of B into geopolymers

A combination of leaching experiments and NMR analysis reveals that adding boric acid to alkali-activated geopolymers leads to the conversion of BO<sub>3</sub> to BO<sub>4</sub>, the process enhanced by high-temperature curing. The newly formed BO<sub>4</sub> species preferentially bond to shortrange free Si in the geopolymer, creating asymmetric BO<sub>4</sub>(xB, 4-xSi) structures, while the remaining BO<sub>4</sub> units connect to others B, forming BO<sub>4</sub>(4B, 0Si) structures that exist in an amorphous form outside the primary geopolymer matrix (Fig. 3). Additionally, elevated temperatures promote the substitution of BO<sub>4</sub> for AlO<sub>4</sub>, facilitating its integration into the framework. However, this effect is largely limited to the formation of Si-deficient, unstable BO<sub>4</sub> (xB, 4-xSi) structures. During leaching, nearly all B from the LT group, primarily linked to short-range free Si, is leached out (Fig. 10 (a -1 and -4)). In contrast, the HT group retains a small fraction (<10%) of B after leaching, attributed to the high-temperature promotion of BO<sub>4</sub> substitution for AlO<sub>4</sub> and the relatively higher content of low-aluminium Si tetrahedra in the HT samples, which are rich in Si-O-Si structures. Additionally, boric acid added during acid-activated geopolymerisation can bond with Al-deficient Si tetrahedra (Fig. 6(d)), which form during the dealumination phase (Fig. 5(c)), thereby becoming stably incorporated into the geopolymer framework as symmetric BO<sub>4</sub> (0B, 4Si) structures (Fig. 4(d)). Therefore, no significant leaching of B was observed during the leaching process (Fig. 10(a)).

#### 3.7. Evaluation of immobilisation capacity for radionuclides

The above results show that the acid-activated geopolymers are the most suitable matrix for introducing B by adding boric acid. The impact of introduced B on the radionuclide immobilisation capacity must be evaluated for the implementation of this proposal in radioactive debris. The zeta potential, a key indicator of the electrostatic properties of material surfaces, is crucial for analysing the interactions between geopolymers and charged ions. Fig. 11 shows the zeta potential behaviour of all acid group samples across a pH range from acidic to basic (pH 3-11). After equilibration, a general decrease in solution pH was observed, likely due to the acidic nature of the acid-activator. The zeta potentials of all samples initially rose and then declined as the pH varied, peaking at positive values in neutral solutions with an initial pH of 7. A previous study has revealed that [48], in acid-activated geopolymers, positively charged Al<sub>6</sub> structures are released due to the cleavage of their bridging O-P-O bonds under acidic conditions, leading to a reduction in zeta potential as pH decreases. In alkaline conditions, the decrease in zeta potential is primarily attributed to the deprotonation of Si-OH groups, forming negatively charged Si-O structures, which reduce the zeta potential as the pH increases. In Fig. 11, the rate of pH change in the samples under acidic conditions increased with higher B content, which correlated with the amount of Al<sub>6</sub> (Fig. 5 (d)) and the higher near-Si terminal P in the framework (Fig. 7). The peak zeta potential of the samples decreased progressively with increasing B content, in contrast to the results of positively charged Al6 content. This is because the introduced B bond to the framework in the form of BO<sub>4</sub>, which is structurally similar to its group counterpart AlO<sub>4</sub> and carries a negative charge, leading to a reduction in the overall positive charge as the B content increased. In alkaline conditions, the negative change rate of zeta potential decreased as B content increased. Zeta potential in these environments is predominantly governed by the Si/(Al + B) ratio, which reflects the relative content of Si tetrahedra. Therefore, the negative change in zeta potential slowed down as the B content increased.

Fig. 12 presents the dynamic leaching results for anionic  $SeO_3^{2-}$  and cationic  $Cs^+$  in acid group samples with varying B contents. It was observed that the samples had a high immobilisation capacity of >97% for both ions, regardless of B addition. The leaching of  $SeO_3^{2-}$  increased with higher B content (Fig. 12 (a)) due to a reduction in the matrix's positive charge, which weakened its electrostatic adsorption capacity for the anions (Fig. 11). In contrast,  $Cs^+$  leaching slightly decreased as B content increased (Fig. 12 (b)). Previous studies [77] suggest that the immobilisation of  $Cs^+$  in acid-activated geopolymers primarily results from physical entrapment within the dense matrix. Therefore, the

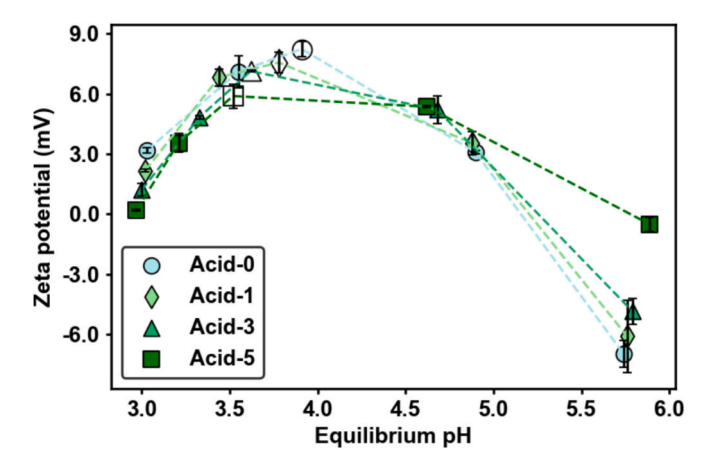


**Fig. 11.** Zeta potential of acid group samples at various pH values after equilibrium (empty symbols identify testing at a pH 7 solution).

reduction in Cs<sup>+</sup> leaching can be attributed to the increased matrix density with B addition. This finding aligns with results from compressive strength tests (Fig. 2), NMR analysis (Fig. 5 (d)), and micromorphology observations (Fig. 8 (c)). The acid-activated geopolymers generally exhibited significant immobilisation capacity for both anionic and cationic radionuclides, with B having a negligible impact.

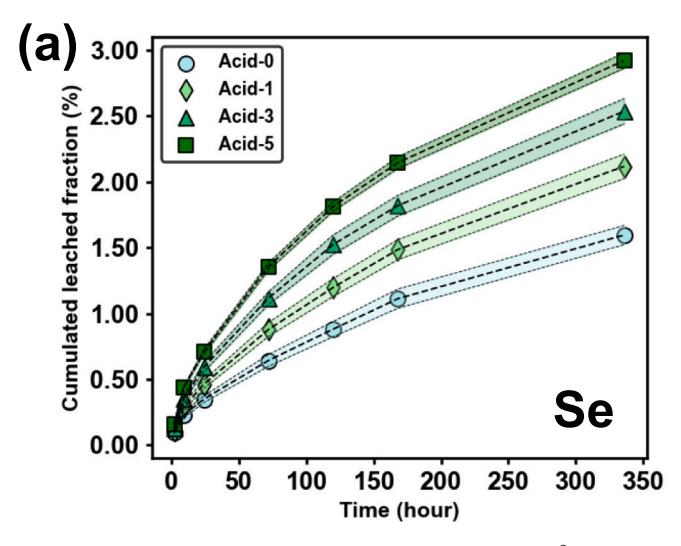
#### 4. Conclusions

The incorporation mechanism and capacity of B into metakaolin-based geopolymers through the addition of boric acid were studied under various activation conditions, including both alkali and acid activators as well as at different curing temperatures. The evaluation of the geopolymers following B incorporation included compressive strength tests, XRD, solid-state MAS NMR, SEM, FTIR, and leaching tests. The radionuclide immobilisation capacity of the acid-activated geopolymer was further assessed through zeta potential measurements and leaching tests. The conclusions are as follows:

- 1) Adding boric acid to alkali-activated geopolymers cured at low temperatures reduced the compressive strength due to the effect on the geopolymerisation. The  $BO_3$  units in boric acid were partially converted into  $BO_4$  units, most of which bond with the free Si tetrahedra outside the framework to form  $BO_4(xB, 4-xSi)$  structures. The remaining  $BO_4$  units bond with B atoms, forming  $BO_4(4B, 0Si)$  structures. These short-range structures exhibited low connectivity to the matrix and readily leached out during the leaching process ( $\geq 98\%$ ).
- 2) Although high-temperature curing reduced the compressive strength of alkali-activated geopolymers, the addition of boric acid had a negligible negative effect. This is because the increased porosity from high-temperature curing is the primary factor dominating compressive strength. Most  $BO_3$  units in the boric acid converted to  $BO_4$  units, forming  $BO_4(4B, 0Si)$  structures with B atoms, while some formed  $BO_4(xB, 4-xSi)$  structures by bonding with extra Si tetrahedra. High-temperature curing also produced more Al-unsaturated Si tetrahedra, incorporating some  $BO_4(xB, 4-xSi)$  into the framework. Consequently, B remained in the matrix during leaching, reducing B leaching compared to low-temperature curing ( $\geq 90\%$ ).
- 3) Adding boric acid to acid-activated geopolymers effectively mitigated the detrimental effects of the significant heat generated during the initial dealumination phase by absorbing this heat through a reaction with phosphoric acid. This process enhanced both the reactivity and compressive strength of the acid-activated geopolymer. The non-ring and partially ring  $BO_3$  units in the boric acid were converted into  $BO_4$  units, which bond with numerous Alunsaturated Si tetrahedra. Most of the boron in the added boric acid was incorporated into the geopolymer framework as stable  $BO_4(0B, 4Si)$ , which was highly resistant to leaching during the leaching process ( $\leq 5\%$ ).
- 4) The addition of boric acid to acid-activated geopolymer increased the content of  $Al_6$  and near-Si terminal P, accelerating the reduction of zeta potential with decreasing pH in acidic conditions. In the alkaline conditions, however, the reduction in Si/(Al + Si) as increasing B content moderated the decline in zeta potential with increasing pH. The introduction of negatively charged BO<sub>4</sub> structures reduced the positive charge in the geopolymer, slightly diminishing the capacity to immobilise the anionic radionuclide  $SeO_3^{2-}$ . Conversely, the introduction of boric acid slightly improved the immobilisation of the cationic radionuclide  $Cs^+$ , as it increased the denseness of the matrix by promoting acid-activated geopolymerisation.

# CRediT authorship contribution statement

Xiaobo Niu: Writing - review & editing, Writing - original draft,



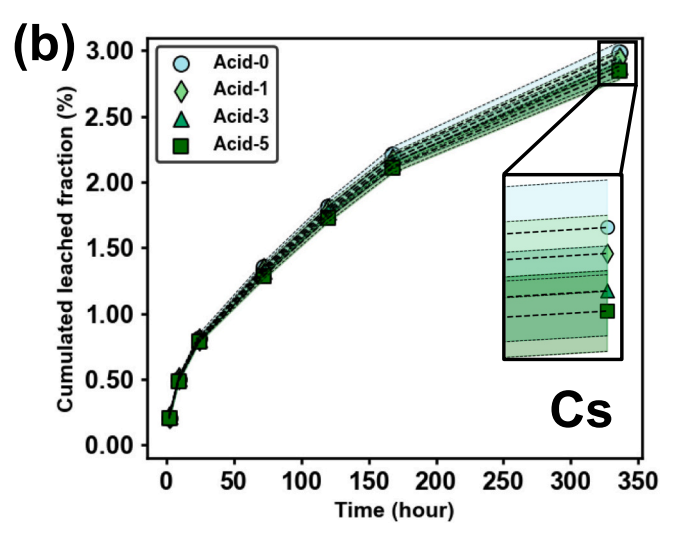


Fig. 12. Cumulative fraction of (a) SeO<sub>3</sub><sup>2-</sup> and (b) Cs<sup>+</sup> leaching from acid group samples as a function of time.

Validation, Methodology, Investigation, Formal analysis, Data curation, Conceptualization. Yogarajah Elakneswaran: Writing – review & editing, Writing – original draft, Supervision, Project administration, Methodology, Funding acquisition, Formal analysis, Conceptualization. Ang Li: Writing – review & editing, Methodology, Investigation, Data curation. Sivasubramaniam Seralathan: Writing – review & editing, Methodology, Investigation, Data curation. Ryosuke Kikuchi: Writing – review & editing, Methodology, Investigation, Data curation. Yoshihisa Hiraki: Writing – review & editing, Supervision, Methodology, Conceptualization. Junya Sato: Writing – review & editing, Supervision, Methodology, Conceptualization. Takeshi Osugi: Writing – review & editing, Supervision, Methodology, Conceptualization. Brant Walkley: Writing – review & editing, Supervision, Methodology, Funding acquisition, Conceptualization.

# Declaration of competing interest

The authors declare that they have no known competing financial interests or personal relationships that could have appeared to influence the work reported in this paper.

### Acknowledgements

JAEA Nuclear Energy S&T and Human Resource Development Project supported part of this work through concentrating wisdom Grant Number R05I121 and EPSRC (UK) under grants EP/Y029208/1. We thank the Instrumental Analysis Support Office, the Frontier Chemistry Center, the Faculty of Engineering, Hokkaido University for allowing us to conduct the analysis using Solid 500 MHz (BRUKER) NMR and for providing insight and expertise that greatly assisted the research. We thank the Sobue Clay Co. Ltd. (Japan) for supporting the raw materials for this study.

### Data availability

Data will be made available on request.

#### References

- TEPCO, Basic Policy for the Contaminated Water Issue at the TEPCO's Fukushima Daiichi Nuclear Power Station. https://www.mofa.go.jp/policy/page3e\_000072. html 2013
- [2] R. Gauntt, D. Kalinich, J. Cardoni, J. Phillips, A. Goldmann, S. Pickering, M. Francis, K. Robb, L. Ott, D. Wang, C. Smith, S. St. Germain, D. Schwieder, C. Phelan, Fukushima Daiichi accident study (status as of April 2012), in: SANDIA REPORT 6173, 2012, https://doi.org/10.2172/1055601.

- [3] T. Kitagaki, H. Ikeuchi, K. Yano, L. Brissonneau, B. Tormos, R. Domenger, J. Roger, T. Washiya, Effect of quenching on molten core-concrete interaction product, J. Nucl. Sci. Technol. 56 (2019) 902–914, https://doi.org/10.2172/1055601.
- [4] H. Takuma, Y. Isao, N. Ryuji, K. Ryunosuke, Preparation of carbonate slurry simulating chemical composition of slurry in overflowed high integrity container and evaluation of its characteristics, JAEA-Technology 012 (2021), https://doi. org/10.11484/jaea-technology-2021-012.
- [5] T. Ikenoue, M. Takehara, K. Morooka, E. Kurihara, R. Takami, N. Ishii, N. Kudo, S. Utsunomiya, Occurrence of highly radioactive microparticles in the seafloor sediment from the pacific coast 35 km northeast of the Fukushima Daiichi nuclear power plant, Chemosphere 267 (2021), https://doi.org/10.1016/j. chemosphere 2020 128907
- [6] G. Steinhauser, Fukushima's forgotten radionuclides: a review of the understudied radioactive emissions, Environ. Sci. Technol. 48 (2014) 4649–4663, https://doi. org/10.1021/es405654c.
- [7] Z. Zhang, K. Ninomiya, Y. Yamaguchi, K. Kita, H. Tsuruta, Y. Igarashi, A. Shinohara, Atmospheric activity concentration of <sup>90</sup>Sr and <sup>137</sup>Cs after the Fukushima Daiichi nuclear accident, Sci. Technol. 53 (2018) 9917–9925, https:// doi.org/10.1021/acs.est.8b01697.
- [8] K. Tanaka, A. Shimada, A. Hoshi, M. Yasuda, M. Ozawa, Y. Kameo, Radiochemical analysis of rubble and trees collected from Fukushima Daiichi nuclear Power Station, J. Nucl. Sci. Technol. 51 (2014) 7–8, https://doi.org/10.1080/ 00223131.2014.921583.
- [9] Y. Koo, Y. Yang, K. Song, Radioactivity release from the Fukushima accident and its consequences: a review, Prog. Nucl. Energ. 74 (2014) 61–70, https://doi.org/ 10.1016/j.pnucene.2014.02.013.
- [10] M. Holt, R.J. Campbell, M.B. Nikitin, Fukushima Nuclear Disaster, CRS Report for Congress, http://171.67.100.116/courses/2017/ph241/kim-d1/docs/R41694.pdf, 2012.
- [11] S. Miwa, Y. Yamamoto, G. Chiba, Research activities on nuclear reactor physics and thermal-hydraulics in Japan after Fukushima-Daiichi accident, J. Nucl. Sci. Technol. 55 (2018) 575–598, https://doi.org/10.1080/00223131.2017.1417177.
- [12] K.N. Prasad, Radiation Injury Prevention and Mitigation in Humans, CRC Press, 2012. https://lccn.loc.gov/2012376391.
- [13] M.M. Weil, J.S. Bedford, H. Bielefeldt-Ohmann, F.A. Ray, P.C. Genik, E.J. Ehrhart, C.M. Fallgren, F. Hailu, C.L.R. Battaglia, B. Charles, M.A. Callan, R.L. Ullrich, Incidence of acute myeloid leukemia and hepatocellular carcinoma in mice irradiated with 1 GeV/nucleon <sup>56</sup>Fe ions, Radiat. Res. 172 (2009) 213–219, https://doi.org/10.1667/RR1648.1.
- [14] A.J. Sigurdson, M. Stovall, R.A. Kleinerman, M.H. Maor, M.E. Taylor, J.D. Boice Jr., E. Ron, Feasibility of assessing the carcinogenicity of neutrons among neutron therapy patients, Radiat. Res. 157 (2002) 483–489, https://doi.org/10.1667/0033-7587(2002)157[0483:FOATCO]2.0.CO;2.
- [15] O. Natalia, I., S. Paul, K. Katya, I. Mohammed, D. Arpitha, H. Kevin P., biomarkers for radiation biodosimetry and injury assessment after mixed-field (neutron and gamma) radiation in the mouse Total-body irradiation model, Health Phys. 115 (2018) 727–742, https://doi.org/10.1097/HP.00000000000000938.
- [16] D.L. Stricklin, J. VanHorne-Sealy, C.I. Rios, L.A.S. Carnell, L.P. Taliaferro, Neutron radiobiology and dosimetry, Radiat. Res. 195 (2021) 480–496, https://doi.org/ 10.1667/RADE-20-00213.1.
- [17] M. Dong, S. Zhou, X. Xue, X. Feng, M.I. Sayyed, M.U. Khandaker, D.A. Bradley, The potential use of boron containing resources for protection against nuclear radiation, Radiat. Phys. Chem. 188 (2021) 109601, https://doi.org/10.1016/j.radphyschem.2021.109601.
- [18] D.P. Mitchell, The absorption of neutrons detected by boron and lithium, Phys. Rev. 49 (1936) 453–458. https://link.aps.org/doi/10.1103/PhysRev.49.453.

- [19] A.K. Suri, C. Subramanian, J.K. Sonber, S.R.Ch. Murthy, Synthesis and consolidation of boron carbide: a review, Int. Mater. Rev. 55 (2010) 4–40, https:// doi.org/10.1179/095066009X1250672166521.
- [20] T.S.R.C. Murthy, J.K. Sonber, K. Sairam, S. Majumdar, V. Kain, Boron-based ceramics and composites for nuclear and space applications: synthesis and consolidation, Handbook of Advanced Ceramics and Composites (2020), https://doi.org/10.1007/978-3-030-16347-1-22
- [21] A.V. Morozov, A.P. Sorokin, S.V. Ragulin, A.V. Pityk, A.R. Sahipgareev, A. S. Soshkina, A.S. Shlepkin, Effect of boric acid mass transfer on the accumulation thereof in a fuel core under emergency modes at NPPs with WMR, Therm. Eng. 64 (2017) 490–495, https://doi.org/10.1134/S0040601517070047.
- [22] M.F. Hawthorne, The role of chemistry in the development of boron neutron capture therapy of Cancer, Angew. Chem. Int. Ed. Engl. 32 (1993) 950–984, https://doi.org/10.1002/anie.199309501.
- [23] M.A. Glinicki, A. Antolik, M. Gawlicki, Evaluation of compatibility of neutronshielding boron aggregates with Portland cement in mortar, Construct. Build Mater. 164 (2018) 731–738, https://doi.org/10.1016/j.conbuildmat.2017.12.228
- [24] M.K.A. Roslan, M. Ismail, A.B.H. Kueh, M.R.M. Zin, High-density concrete: exploring Ferro boron effects in neutron and gamma radiation shielding, Construct. Build Mater. 215 (2019) 718–725, https://doi.org/10.1016/j. conbuildmat.2019.04.105.
- [25] P. Gokul, J.A. Kumar, R. Preetha, S. Chattopadhyaya, K.M. Mini, Additives in concrete to enhance neutron attenuation characteristics – a critical review, Results Eng. 19 (2023) 101281, https://doi.org/10.1016/j.rineng.2023.101281.
- [26] K. Volchek, M.Y. Miah, W. Kuang, Z. DeMaleki, F.H. Tezel, Adsorption of cesium on cement mortar from aqueous solutions, J. Hazard. Mater. 194 (2011) 331–337, https://doi.org/10.1016/j.jhazmat.2011.07.111.
- [27] M. Arbel Haddad, E. Ofer-Rozovsky, G. Bar-Nes, E.J.C. Borojovich, A. Nikolski, D. Mogiliansky, A. Katz, Formation of zeolites in metakaolin-based geopolymers and their potential application for Cs immobilisation, J. Nucl. Mater. 493 (2017) 168–179, https://doi.org/10.1016/j.jnucmat.2017.05.046.
- [28] R.M. Cornell, Adsorption of cesium on minerals: a review, J. Radioanal. Nucl. Chem. 1993 (1993) 483–500, https://doi.org/10.1007/BF02219872.
- [29] P. Duxson, A. Fernández-Jiménez, J.L. Provis, G.C. Lukey, A. Palomo, J.S.J. van Deventer, Geopolymer technology: the current state of the art, J. Mater. Sci. 42 (2007) 2917–2933, https://doi.org/10.1007/s10853-006-0637-z.
- [30] J.L. Provis, Geopolymers and other alkali activated materials why, how, and what? Mater. Struct. 47 (2014) 11–25, https://doi.org/10.1617/s11527-013-0211-
- [31] J.L. Provis, S.A. Bernal, Geopolymers and related alkali-activated materials, Annu. Rev. Mater. Sci. 44 (2014) 299–327, https://doi.org/10.1146/annurev-matsci-070813-113515
- [32] J. Liu, Y. Xu, J. Wang, W. Zhang, J. Ye, R. Wang, The simmobilising performance and mechanism of geopolymer and its derivative materials for high-level radionuclides Cs and Sr: a review, J. Eur. Ceram. Soc. 16 (2024), https://doi.org/ 10.1007/s41779-024-01018-6.
- [33] TEPCO, Contaminated Water Treatment. https://www.tepco.co.jp/en/decommision/planaction/alps/index-e.html, 2023 n.d.
- [34] S.A. Bernal, J.S.J. van Deventer, J.L. Provis, What happens to 5-year-old metakaolin geopolymers? The effect of alkali cation, in: Calcined Clays for Sustainable Concrete 10, 2015, https://doi.org/10.1007/978-94-017-9939-3\_39.
- [35] A. Palomo, A. Fernández-Jiménez, M. Criado, Geopolymers: same basic chemistry, different microstructures, Mater. Constr. 54 (275) (2004) 77–91, https://doi.org/ 10.3989/mc.2004.v54.i275.249.
- [36] Q. Tian, K. Sasaki, Application of fly ash-based geopolymer for removal of caesium, strontium and arsenate from aqueous solutions: kinetic, equilibrium and mechanism analysis, Water Sci. Technol. 79 (2019) 21162125, https://doi.org/ 10.2166/wst.2019.209
- [37] N. Vandevenne, R.I. Iacobescu, Y. Pontikes, R. Carleer, E. Thijssen, K. Gijbels, S. Schreurs, W. Schroeyers, Incorporating Cs and Sr into blast furnace slag inorganic polymers and their effect on matrices properties, J. Nucl. Mater. 503 (2018) 1–12. https://doi.org/10.1016/J.JNUCMAT.2018.02.023.
- [38] H. Lin, J. Zhang, R. Wang, W. Zhang, J. Ye, Adsorption properties and mechanisms of geopolymers and their composites in different water environments: a comprehensive review, J. Wat. Proc. Eng. 62 (2024) 105393, https://doi.org/ 10.1016/j.jwpe.2024.105393.
- [39] Q. Tian, H. Wang, Y. Pan, Y. Bai, C. Chen, S. Yao, B. Guo, H. Zhang, Immobilization mechanism of cesium in geopolymer: effects of alkaline activators and calcination temperature, Environ. Res. 215 (2022) 114333, https://doi.org/10.1016/j. envres.2022.114333.
- [40] X. Niu, Y. Elakneswaran, R.I. Chaerun, J.L. Provis, T. Sato, Adsorption behaviour of simulant radionuclide cations and anions in metakaolin-based geopolymer, J. Hazard. Mater. 429 (2022) 128373, https://doi.org/10.1016/j. ibazmat 2022 128373
- [41] R.I. Chaerun, N. Soonthornwiphat, K. Toda, K. Kuroda, X. Niu, R. Kikuchi, T. Otake, Y. Elakneswaran, J.L. Provis, T. Sato, Retention mechanism of cesium in Chabazite embedded into Metakaolin-based alkali activated materials, J. Hazard. Mater. 440 (2022) 129732, https://doi.org/10.1016/j.jhazmat.2022.129732.
- [42] N. Soonthornwiphat, Y. Kobayashi, K. Toda, K. Kuroda, C.R. Islam, T. Otake, Y. Elakneswaran, J.L. Provis, T. Sato, Encapsulation of Sr-loaded titanate spent adsorbents in potassium aluminosilicate geopolymer, J. Nucl. Sci. Technol. 19 (2020) 1181–1188, https://doi.org/10.1080/00223131.2020.1775717.
- [43] X. Niu, Y. Elakneswaran, R.I. Chaerun, C. Fang, J.L. Provis, T. Sato, Development of metakaolin-based geopolymer for selenium oxyanions uptake through in-situ ettringite formation, Sep. Purif. Technol. 324 (2023) 124530, https://doi.org/ 10.1016/j.seppur.2023.124530.

- [44] J. Davidovits, Geopolymer, Chemistry and Applications, 2008.
- [45] H. Lin, H. Liu, Y. Li, X. Kong, Properties and reaction mechanism of phosphoric acid activated metakaolin geopolymer at varied curing temperatures, Cem. Concr. Res. 144 (2021) 106425, https://doi.org/10.1016/j.cemconres.2021.106425.
- [46] M. Fawer, M. Concannon, W. Rieber, Life cycle inventories for the production of sodium silicates Int, J. Life Cycle Assess. 4 (1999) 207–212, https://doi.org/ 10.1007/BF02970498
- [47] Y.S. Wang, J.G. Dai, Z. Ding, W.T. Xu, Phosphate-based geopolymer: formation mechanism and thermal stability, Mater. Lett. 190 (2017) 209–212, https://doi. org/10.1016/j.matlet.2017.01.022.
- [48] X. Niu, Y. Elakneswaran, Naoki Hiroyoshi, surface chemistry and radionuclide anion immobilisation potential of phosphoric acid-activated metakaolin-based geopolymers, Cem. Concr. Res. 181 (2024) 107549, https://doi.org/10.1016/j. cemconres.2024.107549.
- [49] A. Öz, İ.B. Kara, B. Bayrak, E. Kavaz, G. Kaplan, A.C. Aydın, Characterisation study of geopolymer concretes fabricated with clinker aggregates, Construct. Build Mater. 384 (2023) 131461, https://doi.org/10.1016/j.conbuildmat.2023.131461.
- [50] B. Bayrak, G. Kaplan, A. Öz, E. Kavaz, O. Çelebi, H.G. Alcan, M. Mohabbi, A. C. Aydın, Metakaolin-based geopolymer concretes for nuclear protection: on the perspective of physicochemical, durability, and microstructure, Struct, Concrete 24 (2023) 5641–6841, https://doi.org/10.1002/suco.202200839.
- [51] K. Nishikawa, S. Hashimoto, S. Rossignol, Fabrication of B<sub>4</sub>C hardened body using geopolymer binder with cold reaction sintering and application to neutron shielding, Ceram. Int. 49 (2023) 12750–12757, https://doi.org/10.1016/j. ceramint.2022.12.140.
- [52] Japanese Industrial Standard, Method of test for compressive strength of concrete, JIS A 1108 (2018) 1–5.
- [53] R.M. Mironenko, O.B. Belskaya, V.P. Talsi, V.A. Likholobov, Quadrupolar magic angle spinning NMR spectra fitted using the Pearson IV function, Solid State Nucl. Magn. Reson. 63–64 (2014) 37–41, https://doi.org/10.1016/j.ssnmr.2014.10.001.
- [54] American Nuclear Society, Measurement of the Leachability of Solidified Low-Level Radioactive Wastes by Short-Term Test Procedure. ANSI/ANS-16.1-2003, American Nuclear Society, Illinois, 2004, pp. 1–33.
- [55] Z. Kubba, G.F. Huseien, A.R.M. Sam, K.W. Shah, M.A. Asaad, M. Ismail, M. Md. Tahir, J. Mirza, Impact of curing temperatures and alkaline activators on compressive strength and porosity of ternary blended geopolymer mortars, Case Stud. Constr. Mat. 9 (2018) e00205, https://doi.org/10.1016/j.cscm.2018.e00205.
- [56] N. Ranjbar, A. Kashefi, G. Ye, M. Mehrali, Effects of heat and pressure on hotpressed geopolymer, Construct. Build Mater. 231 (2020) 117106, https://doi.org/ 10.1016/j.conbuildmat.2019.117106.
- [57] B. Kim, B. Lee, C. Chon, S. Lee, Compressive strength properties of Geopolymers from pond ash and possibility of utilisation as synthetic basalt, J. Korean Ceram. Soc. 56 (2019) 365–373, https://doi.org/10.4191/kcers.2019.56.4.03.
- [58] P. Duxson, J.L. Provis, G.C. Lukey, S.W. Mallicoat, W.M. Kriven, J.S.J. van Deventer, Understanding the relationship between geopolymer composition, microstructure and mechanical properties, Colloid Surf. A 269 (2005) 47–58, https://doi.org/10.1016/j.colsurfa.2005.06.060.
- [59] B. Kim, J. Kang, Y. Shin, T. Yeo, W. Um, Immobilisation mechanism of radioactive borate waste in phosphate-based geopolymer waste forms, Cem. Concr. Res. 161 (2022) 106959, https://doi.org/10.1016/j.cemconres.2022.106959.
- [60] F. Angeli, O. Villain, S. Schuller, T. Charpentier, D. de Ligny, L. Bressel, L. Wondraczek, Effect of temperature and thermal history on borosilicate glass structure, Phys. Rev. B 85 (2012) 054110. https://link.aps.org/doi/10.1103/ /PhysRevB.85.054110.
- [61] B. Kim, J. Lee, J. Kang, W. Um, Development of geopolymer waste form for immobilisation of radioactive borate waste, J. Hazard. Mater. 419 (2022) 126402, https://doi.org/10.1016/j.jhazmat.2021.126402.
- [62] M. Zeyer-Düsterer, L. Montagne, G. Palavit, C. Jäger, Combined <sup>17</sup>O NMR and <sup>11</sup>B-<sup>31</sup>P double resonance NMR studies of sodium borophosphate glasses, Solid State Nucl. Mag. 27 (2005) 50-64, https://doi.org/10.1016/j.ssnmr.2004.06.009.
- [63] F. Taulelle, B. Bouchevreaua, C. Martineaua, NMR crystallography driven structure determination: nanoporous materials, Cryst. Eng. Comm. 15 (2013) 8613–8622, https://doi.org/10.1039/C3CE41178H.
- [64] G. Taveri, J. Tousek, E. Bernardo, N. Toniolo, A.R. Boccaccini, I. Dlouhy, Proving the role of boron in the structure of fly-ash/borosilicate glass based geopolymers, Mater. Lett. 200 (2017) 105–108, https://doi.org/10.1016/j.matlet.2017.04.107.
- [65] T. Nanba, M. Nishimura, Y. Miura, A theoretical interpretation of the chemical shift of <sup>29</sup>Si NMR peaks in alkali borosilicate glasses, Geochim. Cosmochim. Ac. 68 (2004) 5103–5111, https://doi.org/10.1016/j.gca.2004.05.042.
- [66] A.R. Grimmer, D. Müller, G. Gözel, R. Kniep, Multinuclear (<sup>11</sup>B, <sup>31</sup>P) MAS NMR spectroscopy of borophosphates, Fresenius J. Anal. Chem. 357 (1997) 485–488, https://doi.org/10.1007/s002160050197.
- [67] L. Munoz-Senovilla, G. Tricot, F. Munoz, Kinetic fragility and structure of lithium borophosphate glasses analysed by 1D/2D NMR, Phys. Chem. Chem. Phys. 19 (2017) 22777–22784, https://doi.org/10.1039/C7CP04171C.
- [68] S. Chen, S. Ruan, Q. Zeng, Y. Liu, M. Zhang, Y. Tian, D. Yan, Pore structure of geopolymer materials and its correlations to engineering properties: a review, Construct. Build Mater. 328 (2022) 127064, https://doi.org/10.1016/j. conbuildmat.2022.127064.
- [69] W.K.W. LeeJ, S.J. van Deventer, Use of infrared spectroscopy to study Geopolymerization of heterogeneous amorphous Aluminosilicates, Langmuir 19 (21) (2003) 8726–8734, https://doi.org/10.1021/la026127e.
- [70] C.A. Rees, J.L. Provis, G.C. Lukey, J.S.J.v. Deventer, In situ ATR-FTIR study of the early stages of fly ash geopolymer gel formation, Langmuir 23 (2007) 9076–9082, https://doi.org/10.1021/la701185g.

- [71] J. Li, Z. Sun, L. Wang, X. Yang, D. Zhang, X. Zhang, M. Wang, Properties and mechanism of high-magnesium nickel slag-fly ash based geopolymer activated by phosphoric acid, Construct. Build Mater. 345 (2022) 128256, https://doi.org/ 10.1016/j.conbuildmat.2022.128256.
- [72] P.Y. Shih, S.W. Yung, T.S. Chin, FTIR and XPS studies of P<sub>2</sub>O<sub>5</sub>-Na<sub>2</sub>O-CuO glasses, J. Non Cryst. Solids 244 (1999) 211–222, https://doi.org/10.1016/S0022-3093 (99)00011-3
- [73] H.K. Tchakouté, C.H. Rüscher, E. Kamseu, F. Andreola, Cristina Leonelli, influence of the molar concentration of phosphoric acid solution on the properties of metakaolin-phosphate-based geopolymer cements, Appl. Clay Sci. 147 (2017) 184–194, https://doi.org/10.1016/j.clay.2017.07.036.
- [74] N. Goel, N. Sinha, B. Kumar, Growth and properties of sodium tetraborate decahydrate single crystals, Mater. Res. Bull. 48 (2013) 1632–1636, https://doi. org/10.1016/j.materresbull.2013.01.007.
- [75] C. Julien, M. Massot, Annealing studies of fast ion conducting glasses by FTIR microscopy, Solid State Ion. 34 (1989) 269–273, https://doi.org/10.1016/0167-2738(89)90454-2.
- [76] Z. Sun, A. Vollpracht, Leaching of monolithic geopolymer mortars, Cem. Concr. Res. 136 (2020) 106161, https://doi.org/10.1016/j.cemconres.2020.106161.
- [77] G. Tan, Z. Liu, X. Ma, Z. Zheng, G. Zhang, B. Wu, L. Zhang, L. Liu, Phosphoric acid-activated metakaolin-based geopolymer: sOptimising P/A molar ratio to solidify Cs <sup>+</sup> and Sr<sup>2+</sup> in nuclear waste, Nucl. Eng. Des. 424 (2024) 113300, https://doi.org/10.1016/j.nucengdes.2024.113300.